



UNIVERSITY OF POTSDAM
DEPARTMENT OF PHYSICS AND ASTRONOMY

BACHELOR THESIS

Hunting for the progenitors of helium white dwarfs

Henry Willem
Matricule number: 801610

supervised by
Harry Dawson
Prof. Stephan Geier

October 14, 2022

Contents

1 Abstract	2
2 Introduction	3
2.1 Stellar evolution	3
2.2 Binary star systems	6
2.3 Evolution and known population of pre-ELM binaries	8
3 Photometry	12
3.1 Photometric data	12
3.2 Spectral energy distribution of stars	14
3.3 Examples of SED fittings	18
4 Sample selection	20
4.1 Prioritization	23
5 Results	25
5.1 Spectral energy distribution fitting	25
5.2 Mass distributions	29
6 Conclusions/summary	35
7 Kurzzusammenfassung (German)	36
8 References	37
9 Appendix	40
*	

1 Abstract

Pre-ELM (extremely low mass) stars, also known as helium white dwarf (WD) progenitors, are stars having effective temperatures ranging from about 9000 K to 35000 K while their luminosities are way below main sequence stars with similar temperatures. They are in a late evolutionary state.

My task was to find these stars to increase their sample size because there are only few currently known. My work did a selection from a hot subdwarf catalogue from Culpan et al. (2022) containing 6600 hot subdwarfs. Helium-WD progenitors are expected to be primarily located below the EHB (extreme horizontal branch) in the T_{eff} -log g- diagram.

Due to similar spectroscopic properties of pre-ELMs (extremely low mass) and hot subdwarfs, it is mandatory to distinguish them by mass. Masses can be determined by combining the SED (spectral energy distribution) with the parallax distance.

An SED fit was run for 267 stars of the sample and the results were inspected visually to evaluate their validity. With the SEDs I got the opportunity to decide whether the star is a pre-ELM (masses starting from about $0.15 M_{\odot}$) and having an upper bound of $0.5 M_{\odot}$ or a hot subdwarf. The SED fits revealed that 31 of them have masses in this range, six of them were in good agreement with theoretical predictions. 13 of them have higher masses, which makes them qualify to be a low-mass hot subdwarf.

This leads to a discussion why we can observe these stars. A single main sequence star with $0.4 M_{\odot}$ with no external influences would not have reached a late evolutionary state yet, considering the current age of the universe of about 13.8 billion years. It is necessary to consider binary interactions to explain their existence. The later helium white dwarf progenitor loses mass to the companion until a helium-rich core is left.

2 Introduction

2.1 Stellar evolution

Stars are not keeping their properties such as effective temperature, radius or chemical composition for their whole lives - they evolve. The way how this evolution looks like and how long it takes from birth to death depends of several parameters, especially the mass.

Stellar lifespans. Stellar lifespans can be estimated with equation 1 below.

$$t \sim 10^{10} \left(\frac{M}{M_{\odot}} \right)^{-2} \text{ y.} \quad (1)$$

Therefore, a star with about $30 M_{\odot}$ lives only for about 11 million years. In comparison, the evolution of sun-like stars with $1 M_{\odot}$ takes about 10 billion years. Hence, a star's lifetime primarily depends on its mass.

When a star is born from a gaseous cloud, they are usually located in the main sequence of the Hertzsprung-Russell diagram (HRD) as shown in Fig. 1 as they start burning hydrogen in their core. These stars are called Zero-Age main sequence stars (ZAMSS). The lowest mass a star can have in order to ignite hydrogen burning is $0.08 M_{\odot}$.

The lifetime, as mentioned before, is approximately describing when a star leaves the main sequence because the states later are short-lasting in comparison of being in the main sequence. During the period of a main sequence star, it fuses hydrogen to helium in the core. The star is in a hydrostatic equilibrium where the inward gravitational pressure is equal to the outward radiation pressure.

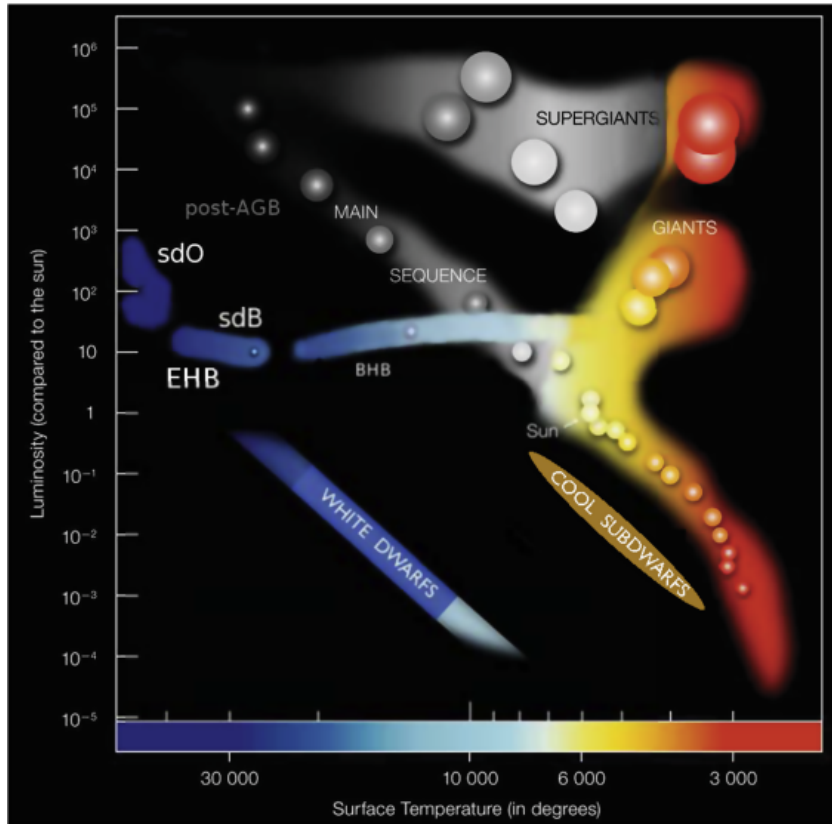


Figure 1: Hertzsprung-Russell diagram (Heber, 2016)

Now it is mandatory to distinguish between how massive the stars are. There are three categories of stellar evolution after the main sequence appearance and they depend on initial mass.

- low-mass stars ($M < 2 M_{\odot}$), whose evolution is explained in detail below.
- intermediate-mass stars ($2 M_{\odot} < M < 8 M_{\odot}$)
- massive stars ($M > 8 M_{\odot}$)

Low-mass stars having masses below $2 M_{\odot}$ have a relatively long lifespan, at least 2.5 billion years (calculated from equation 1).

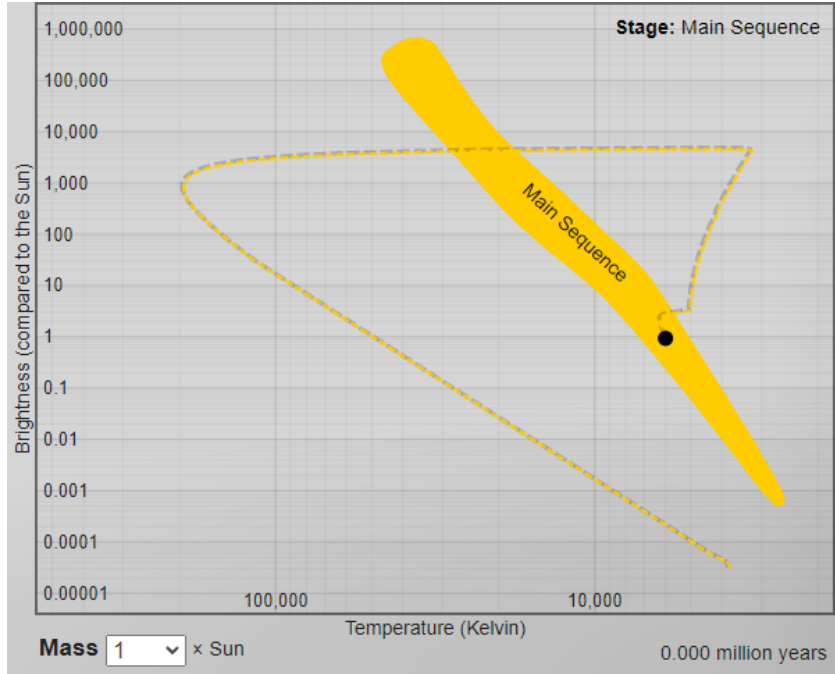


Figure 2: Evolutionary track of a $1 M_{\odot}$ MS star
 created with a simulation Star in a Box <https://starinabox.lco.global>

Evolution of a single $1 M_{\odot}$ star. The single star evolution is well understood. This description is referring to de Boer and Seggewiss (2008). When pressure and temperature from the gaseous cloud are high enough to start hydrogen fusion, the star will get fast ($\sim 10^5$ years) into an hydrostatic equilibrium state and it does not contract more. Then the star is starting its life in the main sequence. A sun-like star stays there for about 10 billion years, as of equation 1.

When the star runs out of hydrogen fuel in its core, it turns into a red giant as hydrogen is then burnt in the shell and it moves into the RGB (red giant branch). Its radius and therefore the luminosity are increasing (Stefan-Boltzmann-law $L = 4\pi r^2 \sigma T_{\text{eff}}^4$). The envelope expands due to efficient energy transport from the core outwards. The star stays in the RGB for about a tenth of the time it was in the main sequence and it loses about 10-40% of its initial mass. The exact amount also depends on the metallicity.

Low-mass stars have a degenerate core. That means that the core is heating up and having an increase in pressure but, unlike ideal gas, it does not expand.

Once the critical mass of $0.5 M_{\odot}$ is reached, the degeneracy will be lifted and the core of helium will ignite explosively, releasing an amount of energy which is equivalent to that of an entire galaxy for a short amount of time.

Stars then burn helium in their core and hydrogen in their envelope. Due to this critical mass, all core-helium burning stars on the HB (horizontal branch) have similar luminosities. The hotter HB stars have ejected more of the hydrogen envelope at the end of the RGB phase whereas the cooler ones remained more of their envelope and are therefore redder. This phase lasts for $\sim 10^{6.5} - 10^{8.4}$ years.

When the helium fusion stops, the star will expand again like prior to the RGB phase and the helium-core burning changes to helium-shell burning. But this time this process is faster and the star's size becomes even bigger while it moves to the AGB (asymptotic giant branch). At the late-AGB phase, the star pulsates thermally, the helium burning is sometimes brighter and sometimes fainter, creating pulsations. The AGB phase is lasting for a few million years. At the end of the AGB phase, fusion processes stop and the star has lost most of its envelope due to thermal pulsations.

After the AGB phase (the post-AGB phase), a $1 M_{\odot}$ star turns into a carbon-oxygen-white dwarf with lower masses ($\sim 0.6 M_{\odot}$) than the star once had at the main sequence.

Intermediate-mass-stars, here considered with masses of $2 M_{\odot} < M < 8 M_{\odot}$ are also turning to red giants after leaving the main sequence and there are not turning to a core-collapse supernova but they evolve to more massive white dwarfs ($\sim 0.7 - 1.4 M_{\odot}$) composed with carbon, oxygen or even heavier elements. Unlike low-mass stars, they do not evolve into the HB because they do not have degenerate cores. *More massive stars* are not important for this work because they go supernova and their remnants are neutron stars or black holes and will not be discussed further.

Helium white dwarfs are having masses of about $0.4 M_{\odot}$ (Heber, 2016). According to equation 1, the lifetime of a single main sequence star with this mass is longer than the age of the universe which is 13.8 billion years. That would imply that a single star with $0.4 M_{\odot}$ has not reached the state of a white dwarf yet.

2.2 Binary star systems

More than half of the stars in the universe are components of binary systems. That can heavily influence the evolution throughout their lives because mass transfer between them is possible and, as already mentioned, the lifespan is depending on the mass of the star. There are some different types of binary systems, characterized by the mass ratios and the distance between the companions.

Due to a very low probability of a star capturing another by gravitation be-

cause of the very high distances between stars, binaries are primarily born from the same gas cloud. They are formed simultaneously and, as the three-body-problem suggests, binaries can also be explained by three stars with similar masses where one of them is being ejected from the system while the other two form a stable system (Sahade et al., 1993).

Then two main sequence stars with similar but mostly unequal masses were born. Firstly, both stars can be in a detached state. That means the stars are not filling their Roche lobes (shown as black lines in Fig. 3, left panel) and there is no mass transfer happening. Both stars will evolve like a single star until the more massive one expands to a red giant.

Secondly, the more massive star can fill its Roche lobe since it evolves faster than the less massive companion and this state is called semidetached. At this state, if not too close, it starts stably transferring mass to the less massive companion and does so for a long time scale. This process is known as the Roche lobe overflow (RLOF). This configuration can be seen in Fig. 3, central panel.

Unstable mass transfer happens when a star overfills its Roche lobe too fast, which then instead of accreted by the companion star, the transferred material is distributed around an common envelope and what we may see then is a contact binary system, which is shown in the right panel of Fig. 3.

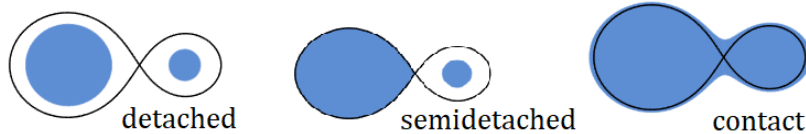


Figure 3: different observable binary configurations
By Philip D. Hall - Own work, CC BY-SA 4.0,

But if a star grows too fast out of its Roche lobe, its mass can be effectively lost from the system, as shown by a simulation¹.

¹<https://demonstrations.wolfram.com/MassTransferInBinaryStarSystems/>

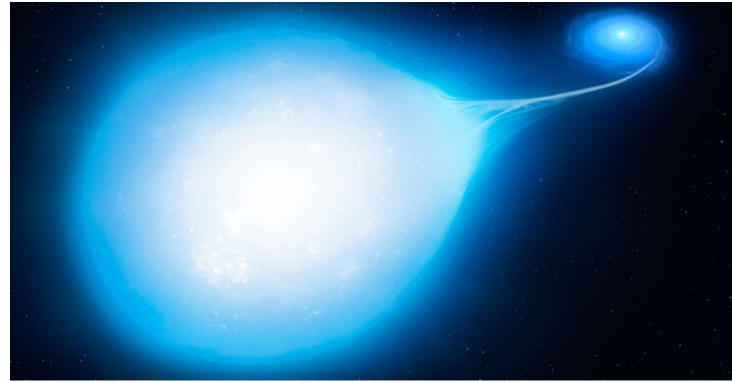


Figure 4: Photo : University of Warwick/Mark Garlick

Mass transfer processes can have strong impacts on both components. This is in fact due to the dependence of the lifetime of a star from its mass.

2.3 Evolution and known population of pre-ELM binaries

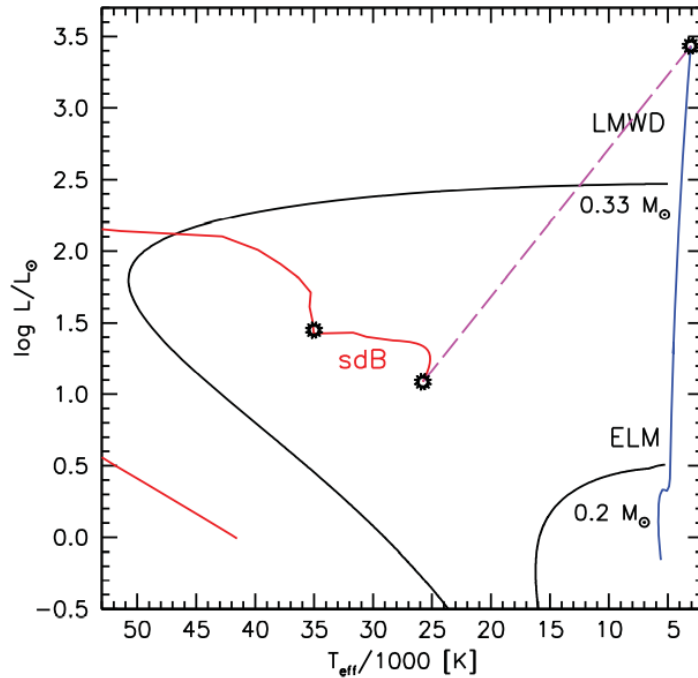


Figure 5: Evolution of pre-ELM white dwarfs with different masses (Heber, 2016)

Different possible evolutionary tracks. Fig. 5 shows the evolution of a sun-like star ($1 M_{\odot}$) starting from main sequence beginning its ascent to the RGB (blue). In a binary system, a sun-like star can lose much of its mass to the companion as the hydrogen envelope being ripped off.

The EHB is the extreme end of the HB. It contains stable core-helium burning stars. The bluer and therefore hotter a star gets, the thinner the hydrogen envelope is. Due to theory of single-star evolution, we are not able to explain this mass loss, so that binary interactions are required to rip off almost the entire hydrogen envelope.

In Fig. 5, these three possible scenarios are shown:

- A core-helium burning extreme horizontal branch (EHB) star (labelled with sdB - subluminous dwarf B)
- A low-mass white dwarf (LMWD) with $0.33 M_{\odot}$
- An ELM (extremely low mass) white dwarf with $0.2 M_{\odot}$.

Firstly, when the hydrogen envelope is removed right at the onset of the helium flash, its $0.5 M_{\odot}$ remains, resulting the formation of an sdB star. Its evolution is shown by the dashed line and it is core-helium burning star starting in the EHB which gets hotter and more luminous, before they eventually cool down and get less luminous.

Secondly, if the hydrogen envelope gets ripped off the star earlier, the helium core has not got enough mass for the flash. The result then is a helium white dwarf. A helium-white dwarf with above $0.33 M_{\odot}$ is called a LMWD and can be formed by low-mass or intermediate-mass stars.

Finally, an ELM helium white dwarf is the result when the hydrogen envelope gets ripped off even earlier. The more massive a white dwarf is, the hotter and more luminous it gets. But the luminosity is never going up, that is because helium-WD progenitors are not burning helium at all. They have masses below $0.33 M_{\odot}$ because even more massive stars can not fuse helium with core masses below $0.33 M_{\odot}$.

Briefly, as you can see from Fig. 5 the evolutionary tracks of hot subdwarfs and helium-WD progenitors are roughly located in the same region of this diagram, thus we expect to find helium-WD progenitors in the hot subdwarf catalogue.

Evolution of pre-ELM stars. Pre-ELM candidates have masses from about $0.15 M_{\odot}$ and they have a maximum mass of roughly $0.5 M_{\odot}$.

Fig. 6 shows theoretical evolutionary tracks of helium white dwarf progenitors for several masses between $0.179 M_{\odot}$ and $0.414 M_{\odot}$ for stars whose

envelope got ripped off before the helium flash as of Driebe et al. (1998) and a known sample from Salaris et al. (2013), shown in black and red dots. The main sequence and the EHB are given as a reference. As you can see here, there are only a few known ones with masses of about $0.25 M_{\odot}$ or above but more of them have masses below $0.2 M_{\odot}$. The more massive a helium-WD progenitor is, the faster they evolve - they become cooler and contract.

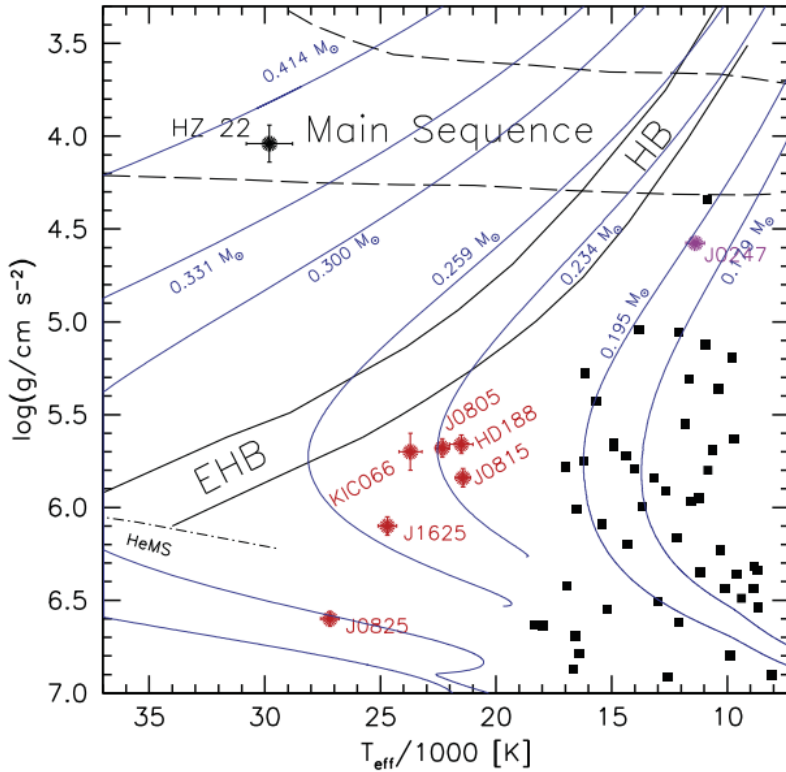


Figure 6: Evolutionary tracks of He-WD progenitors
(Heber, 2016)

Core-helium burning stars. Fig. 6 is also showing the EHB. The EHB contains two lines which are indicating states of helium-burning of hot subdwarfs and the helium flash is happening very suddenly because this process is very temperature sensitive.

- At the zero-age EHB, which is the lower bound of the EHB, an sdB star is starting helium burning.

- At the terminal-age EHB - the upper bound - the sdB star stops helium burning.

In Han et al. (2002), they estimated a subluminous star to stay in the EHB for about 100 million years. This work takes a look at stars from a hot subdwarf catalogue below the EHB because the majority of helium-WD progenitors are expected to be below the EHB according to theoretical evolution models but they can be everywhere throughout the parameter space.

Distinguishing helium white dwarf progenitors from EHB stars. Unlike EHB stars, helium WD-progenitors are not burning helium. Even though they are not related to the EHB but they can be located anywhere in this diagram, as seen from the evolutionary tracks in Fig. 6 . The most important parameter to distinguish between EHB stars from helium-WD progenitors is the mass which is predicted to be lower than EHBs. We need photometric data to determine the mass of the stars. This is done by spectral energy distribution (SED) fitting which is a very important tool for this work.

Known population. HZ 22 was discovered to be a hot subdwarf halo binary (Schönberner, 1978). Heber et al. (2003) have found HD 188112 to be a single He-WD progenitor, which is shown several times later in this work because it is the prototype of this kind of objects.

Pre-ELM stars have even been found as companions of pulsars, e.g. PSR J1012+5307 (discovered by van Kerkwijk et al. (1996)) having a mass of $0.19 \pm 0.02 M_{\odot}$ (Driebe et al., 1998). Even a triple system with a neutron star and *two* white dwarfs was found by Ransom et al. (2014), called PSR J0337+1715. This system is very interesting because there were three phases of mass transfer (even more complex than binaries) and a supernova explosion.

Some other works, listed in Heber (2016), have found a *few* more pre-ELM stars not being companions of pulsars. A list of eight more pulsars with a pre-ELM white dwarf ($M < 0.21 M_{\odot}$) is created by Istrate et al. (2014).

Eclipsing binaries are very useful to have a good constraint for the masses. Hallakoun et al. (2016) found this kind of system with two white dwarfs having masses of $0.38 M_{\odot}$ and $0.23 M_{\odot}$. Six of them were known in 2016 (Heber, 2016) but this work is still relatively up to date (in 2022). CSS 41177 is the only one double-lined eclipsing binary whose radii and masses are constrained with a very high precision (Bours et al., 2014).

Aim of this work. So far, we have explored our current understanding of single-star evolution and how binary interaction can have a strong impact to stellar evolution. I have discussed the implications of ripping of the hydrogen envelope prior to the helium flash which can result of an otherwise inexplicable type of stars.

3 Photometry

This description of Photometry is referring to Heber et al. (2017). Photometry is widely used in stellar astrophysics because this is a powerful tool to determine many properties of stars and the interstellar space such as the spectral class, the effective temperature and interstellar absorption. You have to combine surveys from infrared observation as well as optical and ultraviolet wavelengths to get a complete data set.

Ultraviolet fluxes are used for researching atmospheric properties of a hot sdB star and have been accessed from International Ultraviolet Explorer (IUE), for example, which can be accessed in the MAST archive. Because they are hot with effective temperatures of ranging from 20000 K to 40000 K or even higher, as given from the spectral class, they emit significant amounts of energy in the UV regime.

Observations showed that about one third of sdB stars have cooler main sequence companions. Therefore, there is an expectation of an infrared excess in the spectra as seen in a second bump in the spectra. E. g. these data set were used: ALLWISE, 2MASS and UKIDSS - explained in more detail in the next section.

SDSS and APASS as well as the Subdwarf Database¹ are examples for sources in optical photometry.

3.1 Photometric data

The SED fits are using many data sets from different surveys working in different wavelength regimes as already mentioned in the introduction. Here I am taking a closer look to these surveys.

- Ultraviolet (UV)
 - IUE² provides spectra in the following wavelength ranges: 1150-1975 Å (short UV) and 1915-3150 Å (long UV) which can be

¹<http://catserver.ing.iac.es/sddb/>

²https://www.esa.int/Science_Exploration/Space_Science/IUE_overview

accessed in the MAST¹ archive. Heber et al. (2017) used 1300-1800 Å, 2000-2500Å and 2500-3000 Å to get magnitudes in region of Lyman- α interstellar absorption.

- GALEX² (Galaxy Evolution Explorer; Bianchi et al., 2017) provides data from its NUV and FUV filters. There are sometimes high errors while measuring crowded regions close to the Galactic plane.
- TD-1 was a ESRO satellite providing stellar UV flux data centered at 2740Å, 2365Å, 1965Å and 1565 Å. The catalogue was provided by Thompson et al. (1978).

- Optical

- SDSS (Sloan Digital Sky Survey; Alam et al., 2015),the data release from 2015 covers about 35% of the sky. SDSS provides good coverage in optical wavelengths with five passbands. SDSS was primarily used for faint sources with maximum magnitude of 14.5 like distant galaxies and quasars with long exposure times.
- Gaia (Brown et al., 2018) is giving photometric data in G , G_{RP} and G_{BP} bands.
- Strömgren (Paunzen, 2015), contains narrow u , v , b and y bands and it is optimized for B-,A- and F-type stars. Paunzen (2015) is providing measurements from various data surveys.
- Skymapper (Chiti et al., 2021) provides photometry in u, v, g, r, i and z filters and it is similar to SDSS.
- Hipparcos/Tycho (Høg et al., 2000) has filters for B_t and V_t . The instrument Tycho was installed at the Hipparchos telescope
- PanSTARRS1 (Chambers et al., 2016), an abbreviation for Panoramic Survey Telescope and Rapid Response System, is located on Hawaii and has a wide angle of observation and similar filters compared to SDSS.

- Infrared (IR)

- WISE (Wright et al., 2010), stands for Wide-Field Infrared Survey Explorer, observed all-sky in mid-infrared wavelengths, launched in 2009

¹<https://archive.stsci.edu/>

²<http://www.galex.caltech.edu/about/overview.html>

- VISTA (Visible and Infrared Survey Telescope for Astronomy; Sutherland et al., 2015) is a 4m-telescope located in Paranal, Chile which was used to cover the southern sky in near-IR (wavelengths from 0.8 to 2.3 microns) with some large-area surveys.
- 2MASS¹ (Skrutskie et al., 2006) Two Micron All Sky Survey, providing near-IR data from the whole sky, obtained by two telescopes located in Arizona and Chile. The survey contains I, H and K filters.
- UDKIDSS² (Dye et al., 2006) has a wide-field camera and is a ultra-deep field IR survey within the Y, J, H, Z and K band.

This list of surveys was taken from Dawson (2021).

3.2 Spectral energy distribution of stars

This photometric data which is taken from literature mentioned above is used to obtain a spectral energy distribution (SED). SEDs are a powerful tool to identify binary star systems containing an sdO or sdB star with a cool companion star.

These six parameters are part of the model which are simulating the SED (Heber et al., 2017):

- Angular diameter Θ (fitted)
- Effective temperature T_{eff} (prescribed)
- Surface gravity $\log g$ (prescribed)
- Helium abundance $\log n((He))/\log n((all))$ (fixed)
- Metallicity z (fixed)
- Interstellar reddening parameter $E(B - V)$ (fitted)

The interstellar reddening is a fitted parameter in the SEDs. It has a significant impact, especially in shorter wavelengths. Interstellar matter mainly consists of dust particles whose sizes are in order of μm and shorter wavelengths are more scattered than longer wavelengths. Stars have a more reddened appearance than they actually are. Fig. 7 illustrates this.

¹<https://web.archive.org/web/20000526160543/http://pegasus.astro.umass.edu/>

²<http://wsa.roe.ac.uk/>

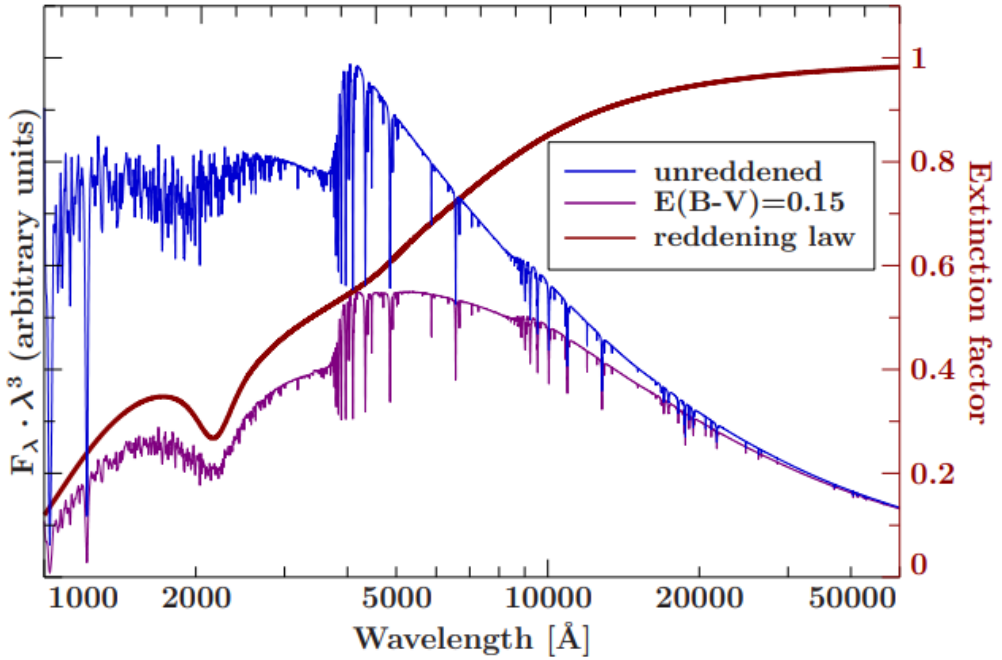


Figure 7: Impact of interstellar reddening (Fitzpatrick, 1999) to SED fitting (Heber et al., 2017)

The values of T_{eff} and $\log g$ have been collected in the catalogue of Culpan et al. (2022). Precisely, there are various literature sources where they came from (see also table 1). The aim is to determine the mass of the stars with these (now fixed) values with this formula:

$$M_* = \frac{gR^2}{G} \quad (2)$$

G is the gravitational constant, R is the radius of the star which can be calculated from the angular diameter Θ and the parallax $\bar{\omega}$ and g is the gravitational acceleration at the surface. This equation states the importance of proper measurements of $\log g$ because small errors can result in heavy impacts to the calculated mass which is very important to find He-WD progenitors.

In spite of being squared, the radius is well constrained in measurements as it moves the SED fit up or down. The sketch in Fig. 8 shows how to convert the parallax and the angular diameter to the radius R to substitute this in equation (2):

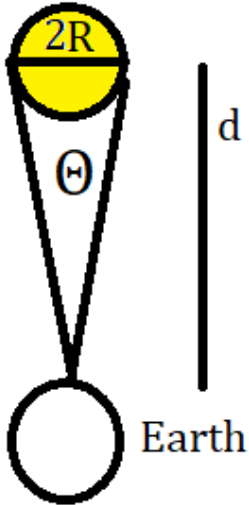


Figure 8: Sketch for the determination of a star's radius

The angular diameter can be determined by $\Theta = 2 \cdot R/d$.

Fitting process. The script is firstly looking in data archives, as listed before, for obtaining photometry. Then it creates synthetic photometry and it fits these to the queried photometric data. The synthetic photometric data flux $F(\lambda)$ is from the star's surface but we are observing it from Earth, a distant point of view, called the received flux $f(\lambda)$.

For decreasing computational time, the synthetic fluxes are taken from a predefined *grid* of model spectra. They contain wavelengths from 300 Å to 10000 Å, effective temperatures from 14000 to 56000 K and surface gravities from 4.8 to 6.2 as they are typical for hot subdwarfs.

This scaling from $F(\lambda)$ to $f(\lambda)$ is done during the fitting process. Assuming spherical symmetry of stellar fluxes, the star's surface fluxes can be calculated with $f(\lambda) = \Theta^2 F(\lambda)/4$.

From this, one gets the magnitude of a star in a specific filter x

$$\text{mag}_x = -2.5 \log \left(\frac{\int_0^\infty r_x(\lambda) f(\lambda) \lambda d\lambda}{\int_0^\infty r_x(\lambda) f^{\text{ref}}(\lambda) \lambda d\lambda} \right) + \text{mag}_x^{\text{ref}}. \quad (3)$$

$r(\lambda)$ indicates the response function, obtained by the transmission of the filter. Zero-points, as mostly defined from Vega (α Lyr) are needed and for this, you have f^{ref} for the flux and $\text{mag}_x^{\text{ref}}$ for the magnitude. The reddening is taken into account by introducing a factor $10^{-0.4A(\lambda)}$ for specific wavelengths. This script is used to minimize χ^2 for finding the best fit in the multi-parameter space.

Some systems have an infrared excess. If this is the case, the script is not fitting a single star but a binary system with two models, mainly composed by a hot subdwarf with a cool companion star. These stars are so close together that it is not possible to resolve both components. Instead, we are measuring the combined flux, shown in black. Fig. 9 shows a binary SED fit. The blue line comes from a hot subdwarf and the red one is a cool companion. Normally, the IR excess is not that obvious to see but the fluxes are multiplied by λ^3 , in order to get a better visualization of the IR excess.

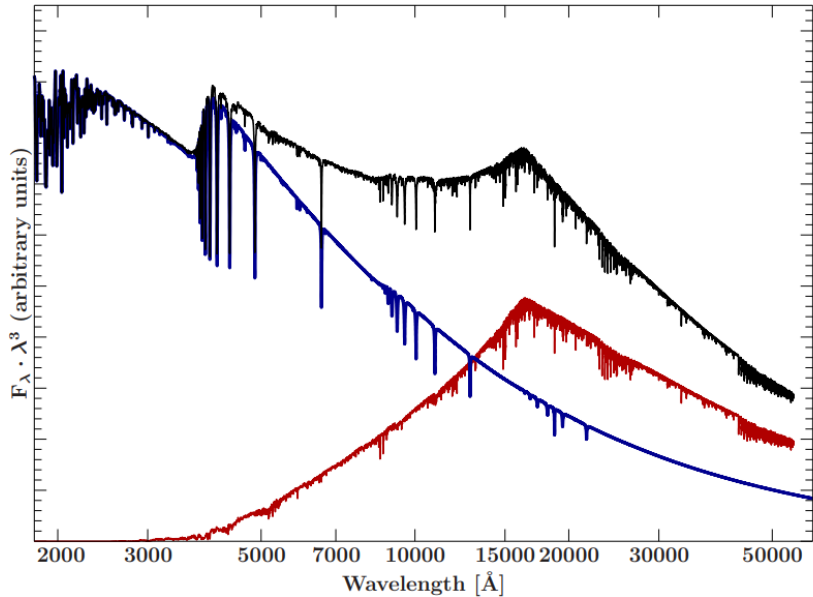


Figure 9: Binary SED fit with IR excess
(Heber et al., 2017)

However, an infrared excess does not necessarily mean that there is a binary system. Infrared excesses can also be caused by a hot disc surrounding a single star which emits IR radiation.

3.3 Examples of SED fittings

- Single hot subdwarfs

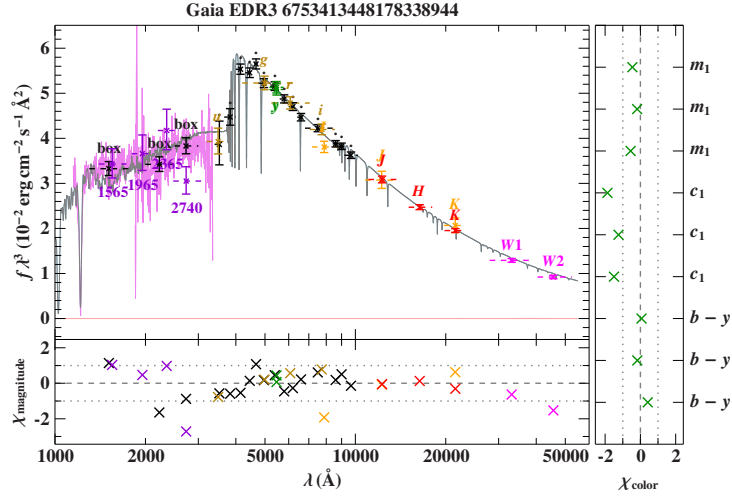


Figure 10: SED fit of HD 188112

HD 188112 is the prototype of sdB-type helium white dwarf progenitors discovered by Heber et al. (2003). Looking at the SEDs is evaluating the quality of the fit. Some other stars can be classified as hot subdwarfs which have a steeper slope in optical and infrared wavelengths. I am showing HE 2135-3749 as an example:

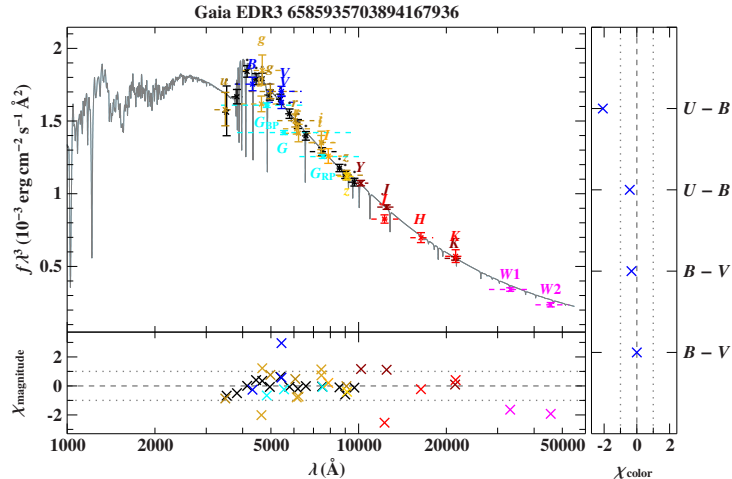


Figure 11: SED fit of HE 2135-3749

- *Composite binary systems*

At some other systems the SED fits a binary system with a hot subdwarf star and a cool companion. An example for this is PG 0749+658:

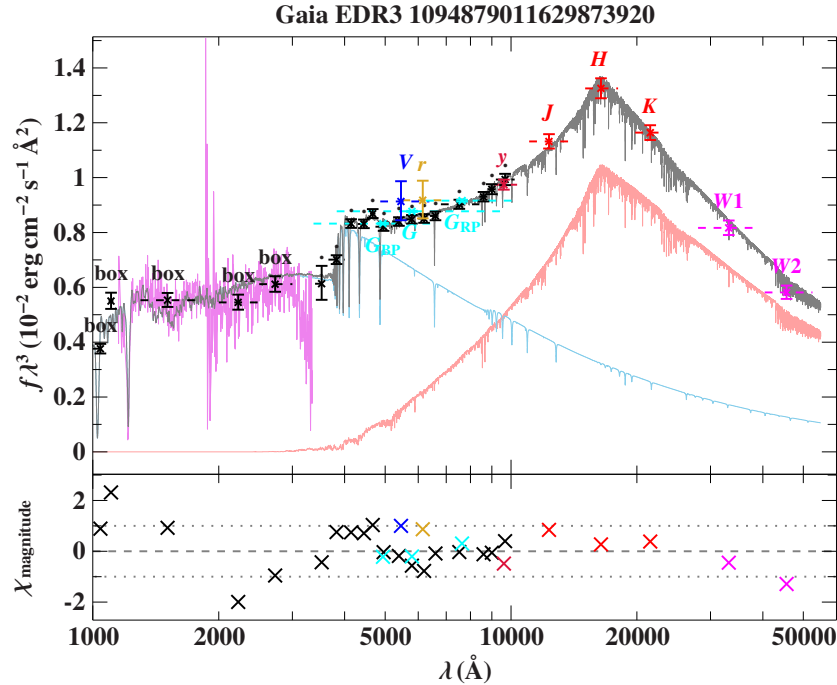


Figure 12: SED fit of PG 0749+658

As one can clearly see, there is an infrared excess in the combined photometric data (grey). If that is detected, the script fits a secondary star (red) to match the overall photometric data. Due to limited resolution of photometric data, the components can not be seen separately in the SED fits.

- *Highly reddened single hot subdwarfs*

The remaining stars are very reddened which causes very low UV fluxes. SDSS J060125.52+224446.3 is an example to show this, the fitted color excess E(44-55) is $0.483^{+0.006}_{-0.088}$ mag.

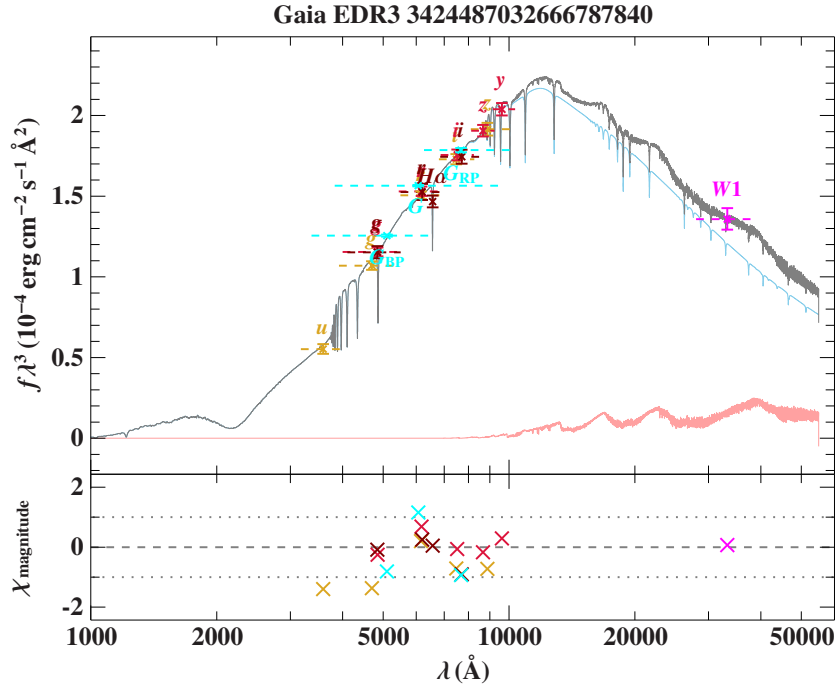


Figure 13: SED fit of SDSS J060125.52+224446.3

We are not only expecting sdB stars in the catalogue because a spectral classification has not been done for all stars in here. Some systems have to be checked further for confirmation of being just reddened or a real contaminator.

4 Sample selection

The catalogue provided by Culpan et al. (2022) from which I am selecting my targets contains spectroscopic parameters like effective temperature, surface gravities and helium abundances. These data was taken from different literature sources. This catalogue is mainly used to identify and classify hot subdwarf stars. For the removal of missclassified objects, they used color indices. Some of them were found by crossmatch with the SIMBAD¹ database. Figs. 14 & 15 are giving an overview of the effective temperatures ($3e4$ means $3 \cdot 10^4$ K) and the decadic logarithms of the gravitational acceleration at the surface (in cm/s²) of the sample where I am taking a look at.

The stars in-between the yellow and the green line are representing the EHB. To be more precise, the green line shows the zero-age EHB und the yellow

¹<http://simbad.cds.unistra.fr/simbad/sim-fbasic>

one indicates the terminal-age EHB. Both lines are based of models taken from Han et al. (2002). Furthermore, the blue line at the bottom is separating the regions where stars do not ignite helium burning according to current models (located to the right) and stars with helium burning to the left. It corresponds to a helium-core mass of $0.35 M_{\odot}$. Additionally, the grey curve is indicating the Helium Main Sequence (HEMS) at which stars are purely composed of helium. The thickness of the hydrogen envelope is increasing with the distance from the HEMS, going upwards.

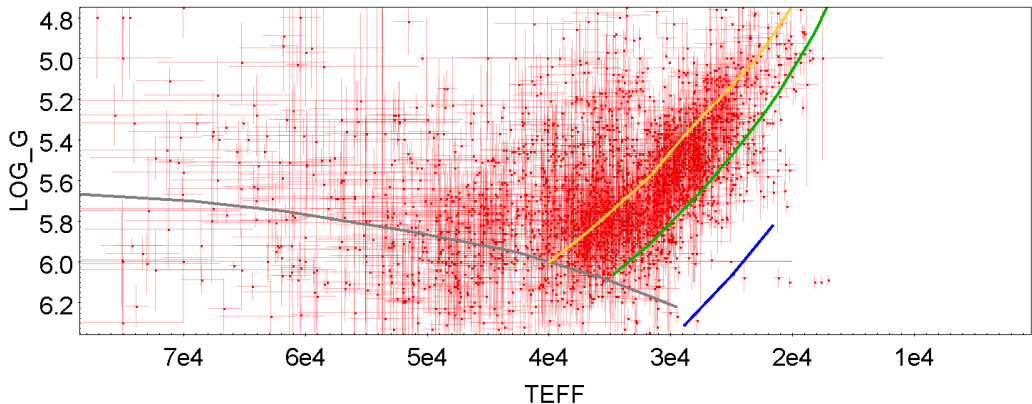


Figure 14: Plot of the T_{eff} – $\log g$ data taken from the catalogue of Culpan et al. (2022)

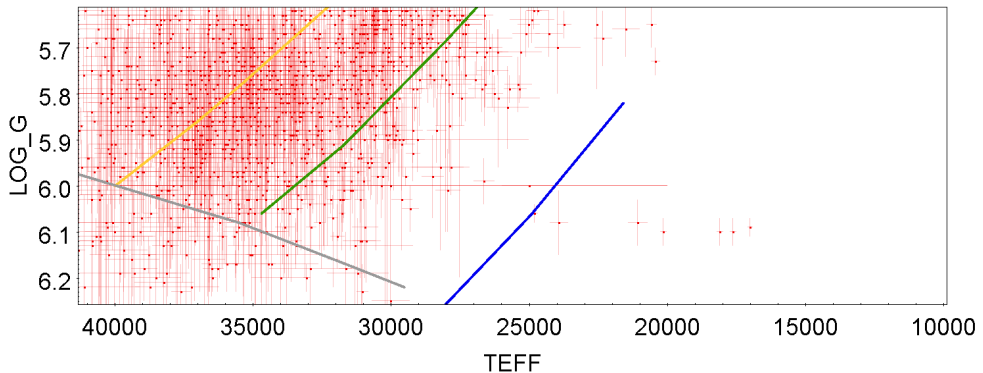


Figure 15: Graph of the data from Culpan et al. (2022) zoomed in

Taking a closer look. Potentially interesting candidates for He-WD progenitors are predicted to be located in the region between the green, blue

and grey line, concerning this parameter space, as given from Fig. 6. The contamination of EHB stars is relatively low here and we are not expecting a helium-WD progenitor to be hotter than where the grey and green line intersect.

Another important thing to be considered for choosing a candidate is how likely it is in this region, preferably choosing those which have a small error bar (shown with the red lines) because then the probability of actually being at this position is high.

Selected candidates. Now the task was to select the interesting stars that may be pre-ELM stars. In order to do this I wrote a python program which can be found in the appendix. Its response was a polynomial with a degree of 4 looking like this:

$$f(x) = -7.588 \cdot 10^{-18}x^4 + 8.418 \cdot 10^{-13}x^3 - 3.606 \cdot 10^{-8}x^2 + 0.0007713x - 1.461$$

where $f(x)$ denotes the log g with respect to the effective temperature x . A cubic polynomial which I tried as well was less accurate. A deviation from the points representing the zero-age EHB was still visible there (the scale was the same as in Fig. 16). Polynomials of higher degrees would be getting more and more accurate but the accuracy has already been sufficient for the purpose of cutting off the sample. The regression (green line) and the data points of the zero-age EHB, coming from Han et al., 2002, which are the same as in Fig. 14 and Fig. 15 can be seen in Fig. 16.

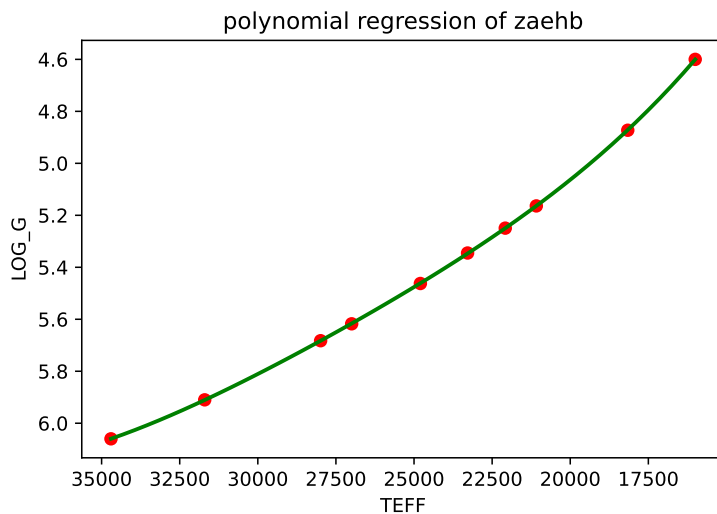


Figure 16: degree-4 polynomial regression of T_{eff} and $\log g$ with zaehb

Fig. 17 shows all of the pre-ELM candidates which are left after the cutting of by the degree-4 polynomial and by the upper bound of the temperature at $T_{\text{eff}} = 34700$ K.

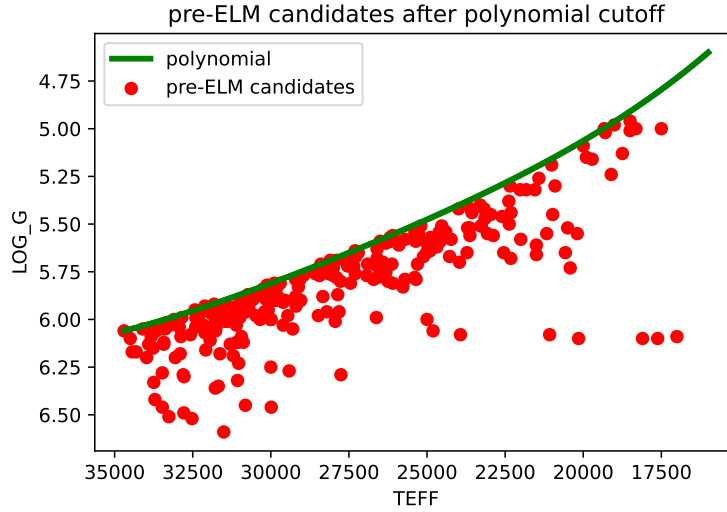


Figure 17: pre-ELM candidates after cutoff

Out of the total catalogue containing 6616 stars, the number of stars left is 267 which is a fraction of about 4%.

Nine of them were excluded later because they are part of an NGC catalogue and these stars are mainly located in globular clusters where the star density is very high.

4.1 Prioritization

There are still over 250 stars in the sample. Therefore, it made sense to do a prioritization.

The main aspect is to consider the probability of the star being in the interesting region (see Fig. 17) below the polynomial regression. All stars have error bars and an appropriate selection can be done in the following way:

- Stars with a higher priority have error bars completely *below* the polynomial so that it is very likely a pre-ELM candidate
- Stars with a lower priority have error bars so that they cross the polynomial cut-off.

After cutting off again with the same borders (the polynomial and effective temperatures $T_{\text{eff}} < 34700\text{K}$) but considering the error bars of the sample this time led to a significant loss of stars, 176 of 267 remained.

There are still some stars with relatively high uncertainties and others with lower ones. I decided to divide the remaining sample into two more sets, distinguished by the value of errors. The set with lower errors contains all stars with an error of $T_{\text{eff}} < 300\text{K}$ and an error of $\log g < 0.15$. These values divide the high-priority-sample in two almost equal subsets (90 out of 176 stars belong to the low-error subset). Fig. 18 is visualising that:

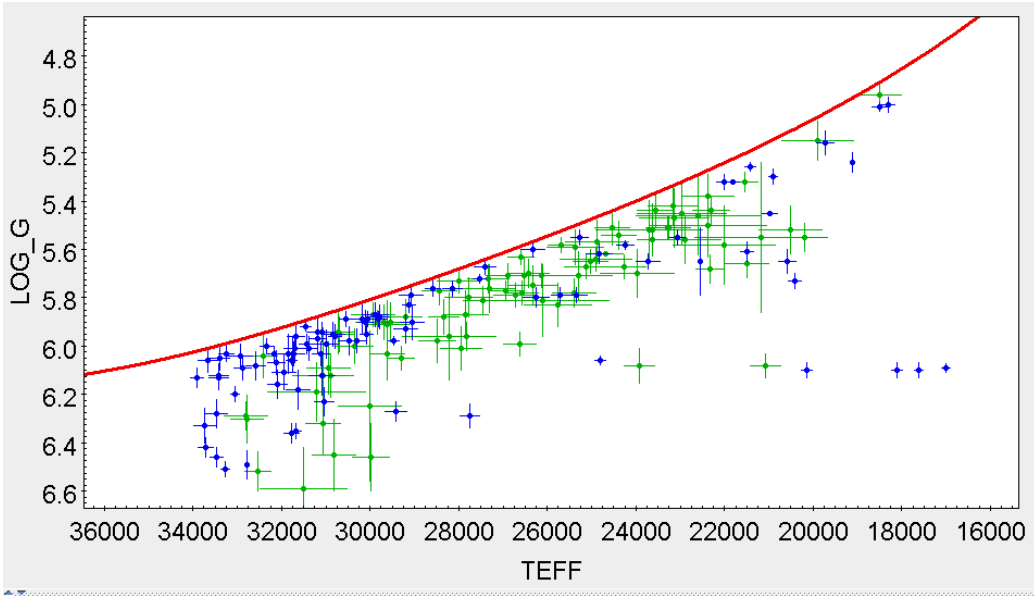


Figure 18: Division of high-prio-pre-ELM candidates according to error bars

The blue stars are belonging to the low-error subset and the others are contributing to a subset with higher error bars. I did this differentiation because the data was obtained in various literature sources. Therefore I want to ensure that the measurements were done properly. When a star has higher error bars you have to be more careful while drawing conclusions according to the measurements.

5 Results

5.1 Spectral energy distribution fitting

After running the SED script for all candidates, I look at the SEDs more carefully. That is important to decide whether the star is a pre-ELM star or something else. I am showing all SEDs from the stars in table 1 in the appendix. For analysing purposes I picked the clean sample as shown in section 3.3.

- There are some stars which are likely *single hot subdwarfs*, e.g. HD 188112 (Fig. 30f) with good data coverage. This star is also fitting quite well with the theoretical prediction in Fig. 23. GD 108 (Fig. 29c) is also a similar example, its SED fit is shown below. But compared to theory, this star is a bit too massive ($0.1 M_{\odot}$).

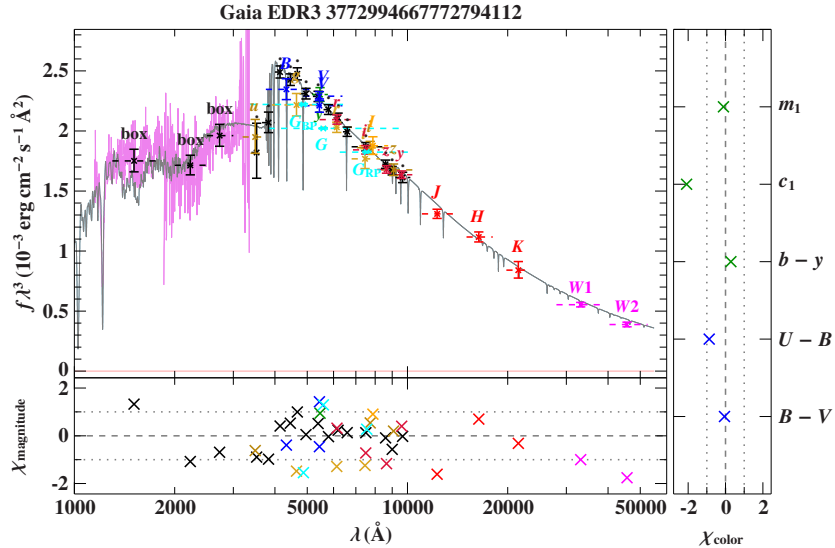


Figure 19: Photometry SED of GD 108

This also applies for:

- KUV02129+2907 (Fig. 27b): Data in visible and IR is very good, some UV surveys would probably validate the status as a He-WD progenitor. It also has a higher mass than expected ($0.31 M_{\odot}$ instead of about $0.24 M_{\odot}$).
- EC 15103-1557 (Fig. 29f): The slope in visible and infrared wavelengths is not so high but UV surveys are missing for validating

the model. This star has $0.29 M_{\odot}$ and about $0.24 M_{\odot}$ would be the prediction.

- UCAC4 576-127603 (Fig. 31c): This star has a relatively high Balmer jump but some UV surveys would be good for being sure. For this star, the difference between calculated and expected mass is $0.1 M_{\odot}$.
- EVR-CB-001 (Fig. 29b) has good coverage of data. Despite of a lack in UV, this star is probably a He-WD progenitor. Here, the Mass from SED fitting is $0.08 M_{\odot}$ higher than the closest line according to evolutionary tracks.
- TON 263 (Fig. 30a): This model looks promising for a He-WD progenitor. But - compared to other stars in this list - more surveys are needed for secure decision. The difference between calculated and predicted mass is smaller, about $0.04 M_{\odot}$.
- PG 2208+014 (Fig. 31d) is well covered in UV, optical and near-IR. The slope is not that high and the Balmer jump is covered too. Only far-IR surveys are needed for a complete SED. Unlike many other stars, the predicted mass is higher than the mass from SED fitting, $\Delta M \approx 0.04 M_{\odot}$.
- PHL 412 (Fig. 31f) is well-known in visual and near-IR. Some UV observations are necessary to confirm the status as a He-WD progenitor but the model looks promising. But the mass difference (calculated-expected) is relatively high, about $0.13 M_{\odot}$.
- Feige 109 (Fig. 32a) is possessing some surveys in optical (but without u band) and infrared and the model looks quite good. Yet there are UV surveys to be made to confirm it. The predicted mass is $0.07 M_{\odot}$ lower than the calculated mass.
- PG 0212+2311.5 (Fig. 27a): There are lots of surveys in visible as well as the u band, and IR wavelengths but it does not have more UV data. Predicted and calculated mass differ by about $0.07 M_{\odot}$ with the calculated mass to be bigger.
- HE0321-0918 (Fig. 27e): This SED fit is looking very similar to the one of PG 0212+2311.5, but it has no u band. The predicted and calculated mass agree here perfectly.
- HE0539-4246 (Fig. 28a) is comparable to PG 0212+2311.5 though the calculated mass is $0.1 M_{\odot}$ higher than you would expect according theoretical models.

- HE 2135-3749 (Fig. 31a) has a relatively steep slope and good coverage in optical and IR regimes. The mass is about $0.1 M_{\odot}$ higher than expected.
- GALEX J080510.9-105834 (Fig. 29a) has good data for infrared and optical wavelengths. Calculated and expected mass differ by $0.16 M_{\odot}$, a very high value.
- KUV 07528+4113 (Fig. 28f) has good coverage in UV and visual (including the u band). Some IR surveys would be needed to be sure. In principal, predicted mass due to its position in the diagram and the calculated mass match, the difference of $0.02 M_{\odot}$ is within the mass error.
- UCAC4 495-061720 (Fig. 29e) is well-known in optical and infrared. Some UV surveys are needed to get a validation. Both expected and calculated mass have a good match.
- SBSS 1709+535 (Fig. 30c) has good data for optical and infrared wavelengths, even though the u band is not looking as good as other bands. Some UV observations would be good for validating the fitted model. Calculated and predicted mass differ by $0.11 M_{\odot}$ while the mass from the SED fit is higher.
- GALEX J173812.4+263408 (Fig. 30d) is very similar-looking to the fit of SBSS 1709+535 and the mass from SED fitting is $0.14 M_{\odot}$ higher than the mass according to theoretical models.
- Other SED fitting are showing a *binary* character such that a hot subluminous star and a cool companion is fitted. Some examples for this are:
 - HE0306-0309 (Fig. 27c): The SED fits a binary system with a hot subdwarf and a cool companion which is not giving much contribution to the total spectra. Calculated and predicted mass match well here.
 - PG 0749+6581 (Fig. 28e): Good coverage of spectral data from UV to IR, the peak is located at the H band, mostly contributed by a cool companion here. The shorter wavelengths are dominated by the hot subluminous star. The mass calculated from SED fit is $0.09 M_{\odot}$ higher than the prediction from the model.
 - PG 1104+476 (Fig. 29d): This cool companion has not a high contribution to the total spectra, which is mainly coming from the hot subdwarf. The calculated mass here is $0.09 M_{\odot}$ bigger than the mass you would expect in this location.

- LAMOST J165809.14+214046.4 (Fig. 30b) is well known in visual wavelengths and has a far-infrared survey as well. An infrared excess was detected though it is relatively weak. The calculated mass is $0.09 M_{\odot}$ higher than the predicted one
- Some other stars do not have much data. Therefore, it is not possible to safely say that they are helium-WD progenitors. Examples for them are:
 - GALEX J074617.1+061006 (Fig. 28d)

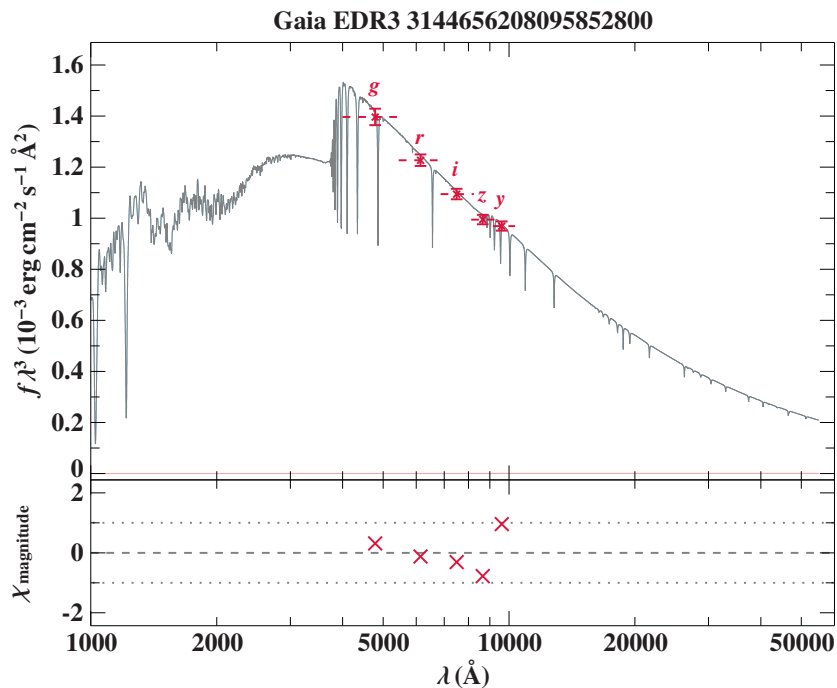


Figure 20: Photometry SED of GALEX J074617.1+061006

This star's mass from SED fit is, additionally, differing from the predicted one by $0.14 M_{\odot}$.

- LAMOSTJ070102.95+094135.6 (Fig. 28c): It only has few data in optical regimes but no UV and IR surveys. Expectation and calculation of its mass match here.
- LAMOSTJ042700.08-025301.6 (Fig. 27f), despite of having a bit more optical data, it is limited in a small wavelength interval, that makes the model not reliable in UV and IR regions. The predicted and calculated masses are matching quite well though.

- SDSS J193756.84+360625.86 (Fig. 30e) has a little bit more data than LAMOSTJ070102.95+094135.6 in optical. There is a difference of about $0.08 M_{\odot}$ while the mass from SED fit was higher.
- SDSS J060125.52+224446.3 (Fig. 28b) has a unusual point for the maximum of $f\lambda^3$ at about 10000 Å. The model fitted a binary system but the cool companion has very small fluxes. Furthermore, the calculated and predicted mass are not matching well because the calculated one is $0.08 M_{\odot}$ bigger.
- SDSSJ031858.70+435539.7 (Fig. 27d) does not have much data, a binary model was fitted but due to lack of UV and IR data, you can not safely say if the model is correct. For this star, theoretical and calculated masses are quite in agreement.
- HE 2150-0238 (Fig. 31b): There are only five surveys in total. Therefore the SED model fit is not very reliable. There is a significant difference between calculation and prediction but lower than many others with only $0.04 M_{\odot}$ with the calculated one to be bigger
- UCAC4 823-026584 (Fig. 31e): Despite of having a bit more data, the uncertainties are relatively high compared to other SED fittings. For a validating purposes, you need more accurate optical and near-IR observations. Additionally, the difference in predicted and calculated mass is rather high ($0.11 M_{\odot}$).

In total, 19 stars have been categorized as single hot subdwarfs, of which six showed good agreement with the theoretical models, defined by $|M_{\text{calc}} - M_{\text{pred}}| \leq 0.04 M_{\odot}$ where M_{calc} is the mass calculated from the SED script and M_{pred} is the mass predicted by the theoretical model from Driebe et al. (1998). Four of them showed a binary character and one of those has a good agreement with the model. For the remaining eight candidates, the spectra coverage was too poor for reliability of the SED fits.

5.2 Mass distributions

After looking at all these stars I chose these that have masses in the following range: $0.15 M_{\odot} < M < 0.5 M_{\odot}$. 31 out of the 267 stars with SED fittings fulfilled this condition with respect to the uncertainties.

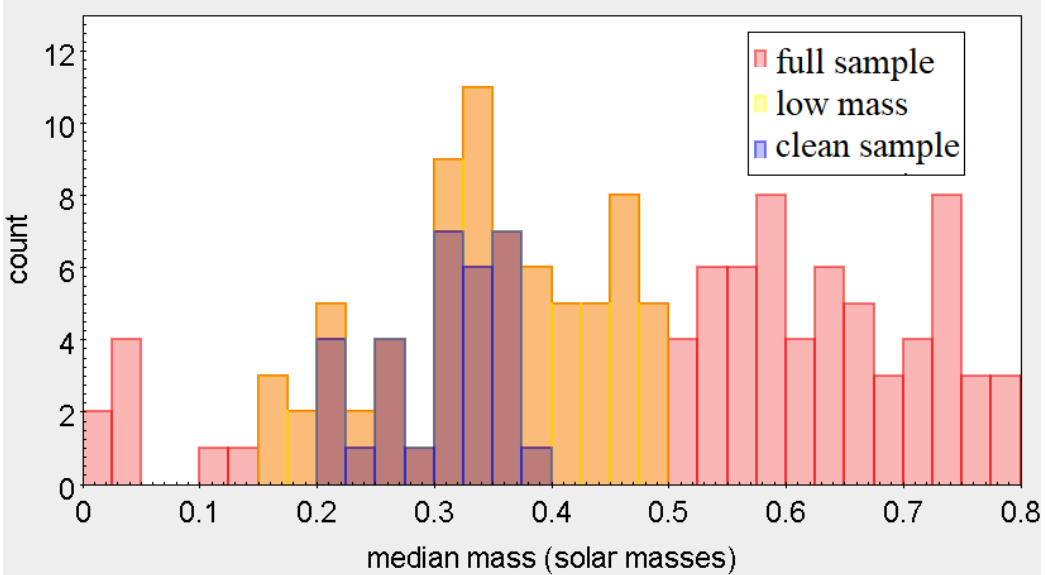


Figure 21: Mass distribution of pre He-WD progenitor candidates

The distribution of the He-WD progenitor candidates within the mass range, even taking their uncertainties into account, is shown by the blue bins and the whole sample has red ones. The yellow sample is showing all stars having interesting median masses but the error bars exceed the interval $[0.15; 0.5]$ M_{\odot} . In total, 73 stars were found to fulfil this condition. That is why some stars having median masses between 0.2 and 0.4 M_{\odot} are excluded for the clean sample. A peak can be seen at $0.35 M_{\odot}$. The clean sample, containing 31 stars and therefore having about half of the selected mass sample, is given in Tab. 1. For the cat. (category) column, g stands for good, b for binary and d for not having much data.

cat.	Name	Parameter reference	median mass [M_{\odot}]
g	PG 0212+231	Luo et al. (2021)	$0.37^{+0.13}_{-0.10}$
g	KUV02129+2907	Luo et al. (2021)	$0.31^{+0.09}_{-0.07}$
g	HE0321-0918	Lisker et al. (2005)	$0.23^{+0.09}_{-0.07}$
g	HE0539-4246	Lisker et al. (2005)	$0.33^{+0.09}_{-0.07}$
g	KUV 07528+4113	Kepler et al. (2019)	$0.22^{+0.10}_{-0.07}$
g	GALEX J080510.9-105834	Németh et al. (2012)	$0.32^{+0.09}_{-0.07}$
g	EVR-CB-001	Ratzloff et al. (2019)	$0.31^{+0.09}_{-0.07}$
g	GD 108	Geier et al. (2013)	$0.35^{+0.10}_{-0.08}$
g	UCAC4 495-061720	Luo et al. (2021)	$0.22^{+0.07}_{-0.05}$
g	EC 15103-1557	Geier et al. (2017)	$0.29^{+0.14}_{-0.10}$
g	TON 263	Geier et al. (2017)	$0.27^{+0.13}_{-0.09}$
g	SBSS 1709+535	Luo et al. (2021)	$0.36^{+0.10}_{-0.08}$
g	GALEX J173812.4+263408	Németh et al. (2012)	$0.37^{+0.10}_{-0.08}$
g	HD 188112	Heber et al. (2003)	$0.22^{+0.06}_{-0.05}$
g	HE 2135-3749	Lisker et al. (2005)	$0.37^{+0.10}_{-0.08}$
g	UCAC4 576-127603	Luo et al. (2021)	$0.33^{+0.09}_{-0.07}$
g	PG 2208+014	Lisker et al. (2005)	$0.21^{+0.07}_{-0.05}$
g	PHL 412	Lisker et al. (2005)	$0.37^{+0.13}_{-0.09}$
g	Feige 109	Geier et al. (2013)	$0.32^{+0.09}_{-0.07}$
b	HE0306-0309	Lisker et al. (2005)	$0.27^{+0.15}_{-0.09}$
b	PG 0749+658	Saffer et al. (1994)	$0.33^{+0.15}_{-0.10}$
b	PG 1104+476	Luo et al. (2021)	$0.24^{+0.13}_{-0.08}$
b	LAMOST J165809.14+214046.4	Luo et al. (2021)	$0.37^{+0.12}_{-0.09}$
d	SDSSJ031858.70+435539.7	Luo et al. (2021)	$0.25^{+0.09}_{-0.07}$
d	LAMOSTJ042700.08-025301.6	Luo et al. (2021)	$0.32^{+0.14}_{-0.10}$
d	SDSS J060125.52+224446.3	Luo et al. (2021)	$0.34^{+0.15}_{-0.13}$
d	LAMOSTJ070102.95+094135.6	Luo et al. (2021)	$0.25^{+0.13}_{-0.08}$
d	GALEX J074617.1+061006	Németh et al. (2012)	$0.39^{+0.11}_{-0.09}$
d	SDSS J193756.84+360625.8	Luo et al. (2021)	$0.34^{+0.10}_{-0.08}$
d	HE 2150-0238	Lisker et al. (2005)	$0.30^{+0.11}_{-0.08}$
d	UCAC4 823-026584	Kupfer et al. (2022)	$0.35^{+0.10}_{-0.08}$

Table 1: List of all stars within mass range $0.15M_{\odot} < M < 0.5M_{\odot}$ (clean sample)

For these stars I took a look of where they are - shown in blue - in the $T_{\text{eff}} - \log g$ -diagram. See also Fig. (17) for the complete sample.

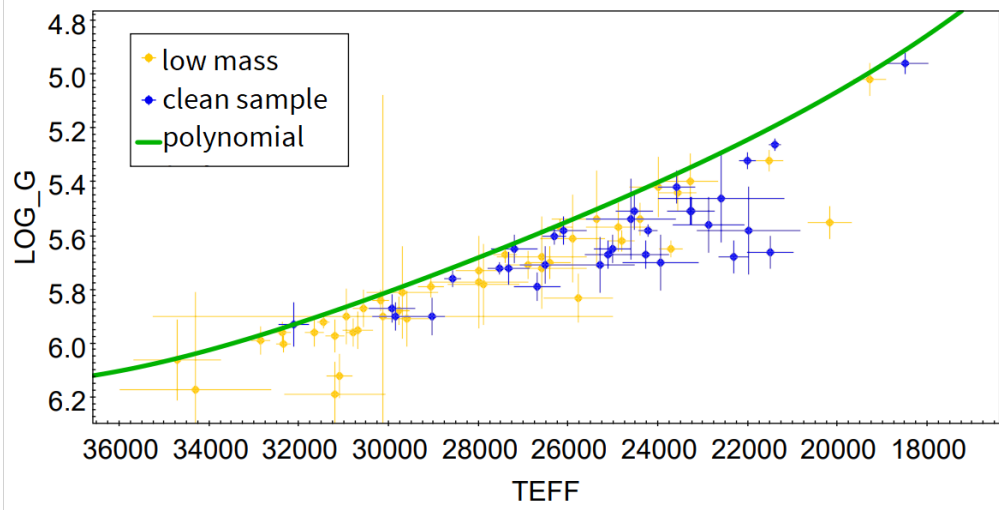


Figure 22: Location of pre-He-WD progenitor candidates with median masses $0.15 M_{\odot} < M < 0.5 M_{\odot}$

The low mass here is meant that a star has a median mass between 0.15 and $0.5 M_{\odot}$ but the uncertainties can reach out of this interval. The clean sample here represents those stars whose uncertainties are within the interval too.

As you can see, most of the pre-ELM candidates with respect to their masses are located not far away from the zero-age EHB. But those which are located further away are less likely associated with the EHB. 26 out of 31 are below the zero-age EHB (green line) even with consideration of the error bars. These stars are in the category "high priority".

Out of these 26 stars, 7 of them have relatively low error bars ($T_{eff} < 300K$ and $\log g < 0.15$) and 19 of these have therefore high error bars, under previously made considerations in section 4.1. Now I am comparing the theoretically predicted masses bases on evolutionary tracks (Driebe et al., 1998):

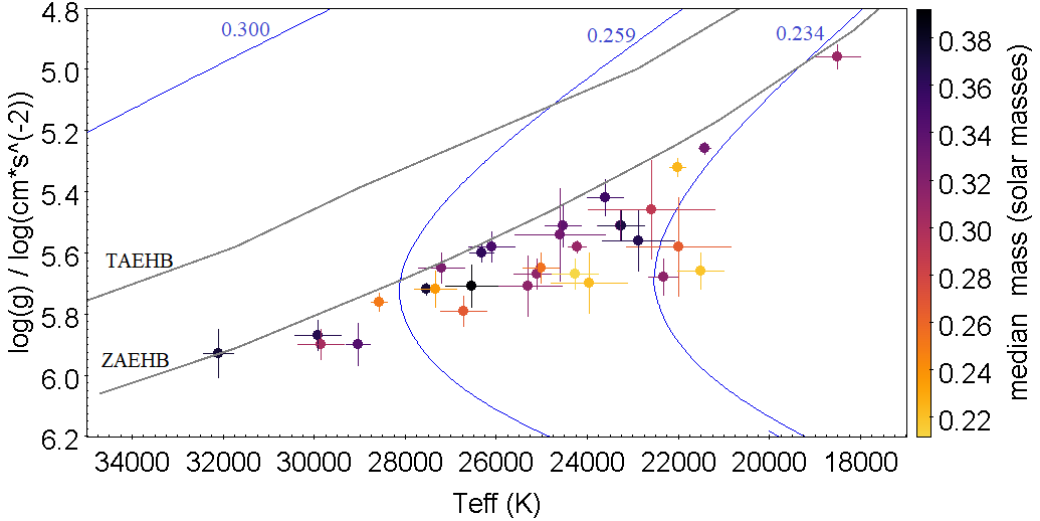


Figure 23: Helium-WD progenitor candidates with evolutionary tracks and coded by mass

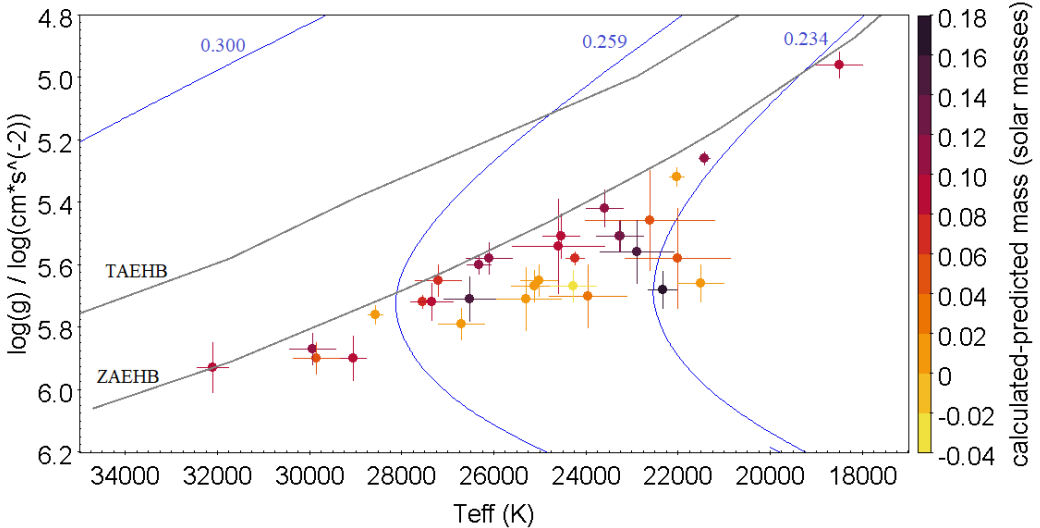


Figure 24: Mass deviations from SED fits compared to theoretical prediction.

Take note of the different meanings of the auxiliary color bars. As you can see in Fig. 23, there is a tendency to higher masses, going left in this diagram. In general, this is what you expect according to the theoretical model because the evolutionary cooling times of more massive stars are shorter. The blue numbers in Figs. 23 & 24 state the mass (in M_{\odot}) for each path which helium-WD progenitors theoretically take. The predicted masses have been

determined by looking at the evolutionary tracks. That allows a simple estimate of the predicted mass by eye. These predicted masses are then compared to the mass I got from the SED fitting. Deviations below 0.04 M_{\odot} are good for validation because the calculated masses always have at least this as an uncertainty. In most cases, the calculated mass from SED fitting was higher than the predicted one. However, only one star showed the opposite - a higher predicted mass.

Also interesting to know is the mass distribution in respect to the surface gravities and to the effective temperatures. Those distributions are shown in the Figs. 25 & 26:

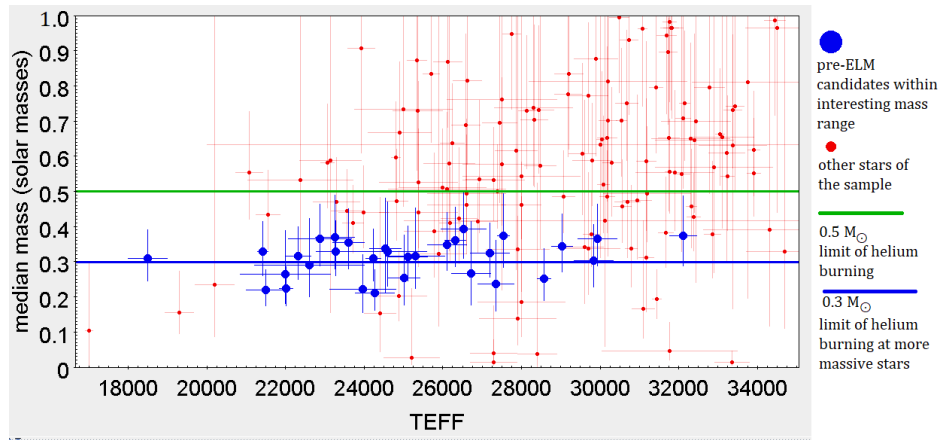


Figure 25: TEFF-median mass diagram

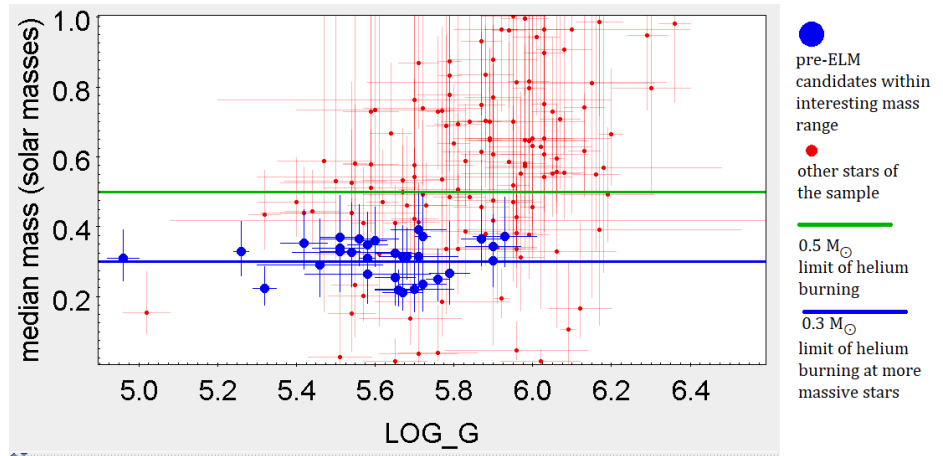


Figure 26: log g-median mass diagram

In these diagrams, some stars can be seen with median masses below $0.5M_{\odot}$ but they are excluded because their error bars are exceeding the limits of $0.15M_{\odot}$ and $0.5M_{\odot}$. As you can see here, the majority of the candidates having median masses between $0.15M_{\odot}$ and $0.5M_{\odot}$, shown in blue, have effective temperatures within a range from roughly 22000 K to 28000 K. The minimum value is 18500 K, the mean is located at 25085 K and the highest effective temperature is 32110 K. The standard deviation is given with $\sigma_{T_{\text{eff}}} = 2926$ K. This is again in agreement with the evolutionary models, predicting less objects with higher temperatures.

The other stars in the sample are rather having higher effective temperatures but the majority of those have too big masses. The SED script has calculated very low masses (lower than $0.1M_{\odot}$ for some stars such that they can not be real stars actually). That is why I introduced the lower bound of $0.15M_{\odot}$ to exclude these objects.

Respectively, the $\log g$ values from the blue stars are ranging between 4.96 and 5.93, having an average of 5.615 and a standard deviation of $\sigma_{\log g} = 0.196$. For higher surface gravities you can see that the calculated masses are increasing as well. That is in agreement with the SED script which uses equation 2 that indicates a proportionality of the mass to the surface gravity.

6 Conclusions/summary

Helium WD-progenitors are stars whose sample size was not so big prior to this work which is a contribution to increase the number of known helium-WD progenitors.

To explain their existence, you need binary interaction with mass transfer as the hydrogen envelope is ripped off prior to the possibility of the helium flash. In fact, a single star with $0.5M_{\odot}$ would not have reached a white dwarf state yet.

Helium WD-progenitors have similar properties compared to hot subdwarfs in the T_{eff} - $\log g$ parameter space. That is the reason why I searched for them in the hot subdwarf catalogue of Culpan et al. (2022). Helium-WD progenitors are likely to be expected below the EHB. In order to exclude contamination of EHB stars, I therefore did a polynomial fit of the zero-age EHB, the lower bound of the EHB, to cut off stars above this line.

267 stars remained and I ran a script creating SED fits for all of these. The SED fit is a powerful tool to determine various properties of stars such as temperature and angular diameter. But the mass is the most important parameter which was used to distinguish Helium-WD candidates from other stars. If the SED fitting detects an infrared excess, it fits two stars - a hot

and a cool component even though a hot disc can also lead to an infrared excess.

Out of the 267 remained stars, 73 (about 26%) have median masses in-between 0.15 and $0.5 M_{\odot}$. 31 stars (11%) are in a clean sample which was defined that the mass errors are within this interval. Afterwards, I took a closer look at the SED fits of the clean sample to find more helium WD-progenitors. I considered 19 stars in total to (likely) be a star of this class. Some other SED fits showed a binary character with two stars. From these systems, future observations can be used to better understand the formation of a helium-WD progenitor.

The remaining systems have to few photometric data - the status of the star can not be safely determined so they need to be observed in more bands in order that upcoming SED fits can be improved.

Additionally, future works should increase the area where you are looking for helium-WD progenitors because they can be even be found in the EHB or above it. But there, the contamination of other stars is very high.

7 Kurzzusammenfassung (German)

In dieser Arbeit ging es vor allem darum, die Anzahl der bekannten Weißen Zwerge aus Helium in einem Frühstadium zu vergrößern. Diese Sterne können nicht als Einzelsterne entstanden sein, da das Alter des Universum dafür nicht ausreicht. Es sind also binäre Interaktionen mit Massentransfer nötig, um deren Existenz zu erklären, wobei die Wasserstoffschale dem Stern vor der Möglichkeit des Helium-Flashes entrissen wurde.

Ich habe mir den Katalog von Culpan et al. (2022) angesehen, da heiße Unterzwerge ähnliche Werte in Schweresbeschleunigung und Effektivtemperatur wie die Helium-Weißen Zwerge haben

Die Kandidaten werden vornehmlich unterhalb des EHB erwartet und daher habe ich alle Sterne darüber herausgenommen. Für diese Sterne habe ich ein Skript laufen lassen, welches verschiedene Parameter wie Temperatur und Winkeldurchmesser bestimmt. Die Masse ist dabei der wichtigste Parameter, da dieser herangezogen wird, um die Helium-Weißen Zwerge von anderen Sternen zu unterscheiden.

Aus den Ergebnissen der SED-Fits habe ich die Kandidaten herausgesucht, die Massen zwischen $0,15$ und $0,5 M_{\odot}$ haben (73). Eine bessere Untermenge hat auch die Messunsicherheiten in diesem Bereich (31). Von diesen 31 Sternen habe ich mir jeden einzelnen SED-Fit angesehen und kam zum Schluss, das es 19 Sterne gibt, die Helium-Weiße Zwerge sind.

Bei manchen Sternen sind aber noch mehr Beobachtungen vonnöten, damit

man den Status als Helium-Weißen Zwerg bestätigen kann. Daher kann die Anzahl dieser Sterne künftig noch weiter gesteigert werden. Zusätzlich sollten künftige Arbeiten den untersuchten Bereich vergrößern, in dem man nach Helium-Weißen Zwergen sucht, da man diese selbst im EHB als auch darüber finden kann, jedoch ist dort die Kontamination von anderen Sternen sehr hoch.

8 References

- Alam et al. (2015). “The Eleventh and Twelfth Data Releases of the Sloan Digital Sky Survey: Final Data from SDSS-III”. English. In: *Astrophysical Journal, Supplement Series* 219. ISSN: 0067-0049. DOI: [10.1088/0067-0049/219/1/12](https://doi.org/10.1088/0067-0049/219/1/12).
- Bianchi et al. (June 2017). “Revised Catalog of iGALEX/i Ultraviolet Sources. I. The All-Sky Survey: GUVcat_AIS”. In: *The Astrophysical Journal Supplement Series* 230.2, p. 24. DOI: [10.3847/1538-4365/aa7053](https://doi.org/10.3847/1538-4365/aa7053). URL: <https://doi.org/10.3847/1538-4365/aa7053>.
- Bours et al. (Mar. 2014). “Precise parameters for both white dwarfs in the eclipsing binary CSS 41177”. In: 438.4, pp. 3399–3408. DOI: [10.1093/mnras/stt2453](https://doi.org/10.1093/mnras/stt2453). arXiv: [1401.1503 \[astro-ph.SR\]](https://arxiv.org/abs/1401.1503).
- Brown et al. (Aug. 2018). “iGaia/i Data Release 2”. In: *Astronomy & Astrophysics* 616, A1. DOI: [10.1051/0004-6361/201833051](https://doi.org/10.1051/0004-6361/201833051). URL: <https://doi.org/10.1051%2F0004-6361%2F201833051>.
- Chambers et al. (2016). *The Pan-STARRS1 Surveys*. DOI: [10.48550/ARXIV.1612.05560](https://doi.org/10.48550/ARXIV.1612.05560). URL: <https://arxiv.org/abs/1612.05560>.
- Chiti et al. (June 2021). “Stellar Metallicities from SkyMapper Photometry. II. Precise Photometric Metallicities of \sim 280,000 Giant Stars with $[Fe/H] < -0.75$ in the Milky Way”. In: *The Astrophysical Journal Supplement Series* 254.2, p. 31. DOI: [10.3847/1538-4365/abf73d](https://doi.org/10.3847/1538-4365/abf73d). URL: <https://doi.org/10.3847/1538-4365/abf73d>.
- Culpan et al. (June 2022). “The population of hot subdwarf stars studied with iGaia/i”. In: *Astronomy & Astrophysics* 662, A40. DOI: [10.1051/0004-6361/202243337](https://doi.org/10.1051/0004-6361/202243337). URL: <https://doi.org/10.1051%2F0004-6361%2F202243337>.
- Dawson (2021). “A Volume-Complete Sample of Hot Subluminous Stars”. MA thesis. Universität Potsdam.
- de Boer, K.S. and W. Seggewiss (2008). *Stars and Stellar Evolution*. EDP Sciences.

- Driebe et al. (Nov. 1998). “The evolution of helium white dwarfs. I. The companion of the millisecond pulsar PSR J1012+5307”. In: 339, pp. 123–133. arXiv: [astro-ph/9809079 \[astro-ph\]](#).
- Dye et al. (Nov. 2006). “The UKIRT Infrared Deep Sky Survey Early Data Release”. In: 372.3, pp. 1227–1252. DOI: [10.1111/j.1365-2966.2006.10928.x](#). arXiv: [astro-ph/0603608 \[astro-ph\]](#).
- Fitzpatrick (Jan. 1999). “Correcting for the Effects of Interstellar Extinction”. In: 111.755, pp. 63–75. DOI: [10.1086/316293](#). arXiv: [astro-ph/9809387 \[astro-ph\]](#).
- Geier et al. (Sept. 2013). “Hot subdwarf stars in close-up view. IV. Helium abundances and the ^3He isotopic anomaly of subdwarf B stars”. In: 557, A122, A122. DOI: [10.1051/0004-6361/201322057](#). arXiv: [1307.5980 \[astro-ph.SR\]](#).
- Geier et al. (Dec. 2017). “Meet the family - the catalog of known hot subdwarf stars”. In: *Open Astronomy* 26.1, pp. 164–168. DOI: [10.1515/astro-2017-0432](#). arXiv: [1711.01856 \[astro-ph.SR\]](#).
- Hallakoun et al. (May 2016). “SDSS J1152+0248: an eclipsing double white dwarf from the Kepler K2 campaign”. In: 458.1, pp. 845–854. DOI: [10.1093/mnras/stw364](#). arXiv: [1507.06311 \[astro-ph.SR\]](#).
- Han et al. (2002). “The origin of subdwarf B stars – I. The formation channels”. In: *Monthly Notices of the Royal Astronomical Society* 336, pp. 449–466.
- Heber et al. (Dec. 2003). “Discovery of a helium-core white dwarf progenitor”. In: 411, pp. L477–L480. DOI: [10.1051/0004-6361:20031553](#).
- Heber (July 2016). “Hot Subluminous Stars”. In: *Publications of the Astronomical Society of the Pacific* 128.966, p. 082001. DOI: [10.1088/1538-3873/128/966/082001](#). URL: <https://doi.org/10.1088/1538-3873/128/966/082001>.
- Heber et al. (2017). *Spectral energy distributions and colours of hot subluminous stars*. DOI: [10.48550/ARXIV.1712.06546](#). URL: <https://arxiv.org/abs/1712.06546>.
- Høg et al. (Mar. 2000). “The Tycho-2 catalogue of the 2.5 million brightest stars”. In: 355, pp. L27–L30.
- Istrate et al. (Nov. 2014). “The timescale of low-mass proto-helium white dwarf evolution”. In: 571, L3, p. L3. DOI: [10.1051/0004-6361/201424681](#). arXiv: [1410.5471 \[astro-ph.SR\]](#).
- Kepler et al. (June 2019). “White dwarf and subdwarf stars in the Sloan Digital Sky Survey Data Release 14”. In: 486.2, pp. 2169–2183. DOI: [10.1093/mnras/stz960](#). arXiv: [1904.01626 \[astro-ph.SR\]](#).

- Kupfer et al. (Feb. 2022). “Discovery of a Double-detonation Thermonuclear Supernova Progenitor”. In: 925.2, L12, p. L12. DOI: [10.3847/2041-8213/ac48f1](https://doi.org/10.3847/2041-8213/ac48f1). arXiv: [2110.11974 \[astro-ph.SR\]](https://arxiv.org/abs/2110.11974).
- Lisker et al. (Jan. 2005). “Hot subdwarfs from the ESO Supernova Ia Progenitor Survey. I. Atmospheric parameters and cool companions of sdB stars”. In: 430, pp. 223–243. DOI: [10.1051/0004-6361:20040232](https://doi.org/10.1051/0004-6361:20040232). arXiv: [astro-ph/0409136 \[astro-ph\]](https://arxiv.org/abs/astro-ph/0409136).
- Luo et al. (Oct. 2021). “Hot Subdwarf Atmospheric Parameters, Kinematics, and Origins Based on 1587 Hot Subdwarf Stars Observed in Gaia DR2 and LAMOST DR7”. In: 256.2, 28, p. 28. DOI: [10.3847/1538-4365/ac11f6](https://doi.org/10.3847/1538-4365/ac11f6). arXiv: [2107.09302 \[astro-ph.SR\]](https://arxiv.org/abs/2107.09302).
- Németh et al. (Dec. 2012). “A selection of hot subluminous stars in the GALEX survey - II. Subdwarf atmospheric parameters”. In: 427.3, pp. 2180–2211. DOI: [10.1111/j.1365-2966.2012.22009.x](https://doi.org/10.1111/j.1365-2966.2012.22009.x). arXiv: [1211.0323 \[astro-ph.SR\]](https://arxiv.org/abs/1211.0323).
- Paunzen (2015). “A new catalogue of Strömgren-Crawford uvbyphotometry”. In: *A&A* 580, A23. DOI: [10.1051/0004-6361/201526413](https://doi.org/10.1051/0004-6361/201526413). URL: <https://doi.org/10.1051/0004-6361/201526413>.
- Ransom et al. (Jan. 2014). “A millisecond pulsar in a stellar triple system”. In: 505.7484, pp. 520–524. DOI: [10.1038/nature12917](https://doi.org/10.1038/nature12917). arXiv: [1401.0535 \[astro-ph.SR\]](https://arxiv.org/abs/1401.0535).
- Ratzloff et al. (Sept. 2019). “EVR-CB-001: An Evolving, Progenitor, White Dwarf Compact Binary Discovered with the Evryscope”. In: 883.1, 51, p. 51. DOI: [10.3847/1538-4357/ab3727](https://doi.org/10.3847/1538-4357/ab3727). arXiv: [1909.02012 \[astro-ph.SR\]](https://arxiv.org/abs/1909.02012).
- Saffer et al. (Sept. 1994). “Atmospheric Parameters of Field Subdwarf B Stars”. In: 432, p. 351. DOI: [10.1086/174573](https://doi.org/10.1086/174573).
- Sahade et al. (1993). *The Realm of Interacting Binary Stars*.
- Salaris et al. (2013). “Comparison of theoretical white dwarf cooling timescales”. In: *A&A* 555, A96. DOI: [10.1051/0004-6361/201220622](https://doi.org/10.1051/0004-6361/201220622). URL: <https://doi.org/10.1051/0004-6361/201220622>.
- Schönberner (Nov. 1978). “The mass of HZ 22.” In: 70, pp. 451–452.
- Skrutskie et al. (Feb. 2006). “The Two Micron All Sky Survey (2MASS)”. In: *The Astronomical Journal* 131.2, pp. 1163–1183. DOI: [10.1086/498708](https://doi.org/10.1086/498708). URL: <https://doi.org/10.1086/498708>.
- Sutherland et al. (Feb. 2015). “The Visible and Infrared Survey Telescope for Astronomy (VISTA): Design, technical overview, and performance”. In: *Astronomy & Astrophysics* 575, A25. DOI: [10.1051/0004-6361/201424973](https://doi.org/10.1051/0004-6361/201424973). URL: <https://doi.org/10.1051%2F0004-6361%2F201424973>.
- Thompson et al. (1978). *Catalogue of stellar ultraviolet fluxes : a compilation of absolute stellar fluxes measured by the Sky Survey Telescope (S2/68) aboard the ESRO satellite TD-1 /*.

- van Kerkwijk et al. (Aug. 1996). “The Masses of the Millisecond Pulsar J1012+5307 and Its White Dwarf Companion”. In: 467, p. L89. DOI: [10.1086/310209](https://doi.org/10.1086/310209). arXiv: [astro-ph/9606045 \[astro-ph\]](https://arxiv.org/abs/astro-ph/9606045).
- Wright et al. (Dec. 2010). “The Wide-field Infrared Survey Explorer (WISE): Mission Description and Initial On-orbit Performance”. In: 140.6, pp. 1868–1881. DOI: [10.1088/0004-6256/140/6/1868](https://doi.org/10.1088/0004-6256/140/6/1868). arXiv: [1008.0031 \[astro-ph.IM\]](https://arxiv.org/abs/1008.0031).

9 Appendix

This python program was used for doing a polynomial regression of the data points representing the zero-age EHB (zaehb)

```
# -*- coding: utf-8 -*-
"""
Created on Tue Jul  5 12:35:25 2022

@author: User
For bachelor thesis
"""

import pandas as pd
import numpy as np
import matplotlib.pyplot as plt

data=pd.read_csv('interestingcandidates.csv')      #reading out data from
                                                    #interesting stars
ehb_han035=pd.read_csv('ehb_han035.csv') #zero-age horizontal branch
hems=pd.read_csv('hems.csv') #helium main sequence
ehb=pd.read_csv('ehb.csv') #zero-age EHB and evolved EHB stars
#converting data to lists

LOG_G=data['LOG_G'].tolist()
e_LOG_G=data['e_LOG_G'].tolist()
TEFF=data['TEFF'].tolist()
e_TEFF=data['e_TEFF'].tolist()
Mass=data['Mass'].tolist()
e_Mass=data['e_Mass'].tolist()
Teff_zaehb=ehb['Teff_zaehb'].tolist()
logg_zaehb=ehb['logg_zaehb'].tolist()
```

```
#polynomial regression
x=Teff_zaehb
y=logg_zae hb
model = np.poly1d(np.polyfit(x, y, 4)) #polynomial fit with degree 4
plt.scatter(x,y)
polyline=np.linspace(16000,34700,50) #start, end, #points
plt.plot(polyline, model(polyline), linewidth=2,color='red')
print(model)
plt.title('polynomial regression of zae hb')
plt.xlabel('TEFF')
plt.ylabel('LOG_G')
ax=plt.gca()
ax.invert_xaxis()
ax.invert_yaxis()
plt.show()
```

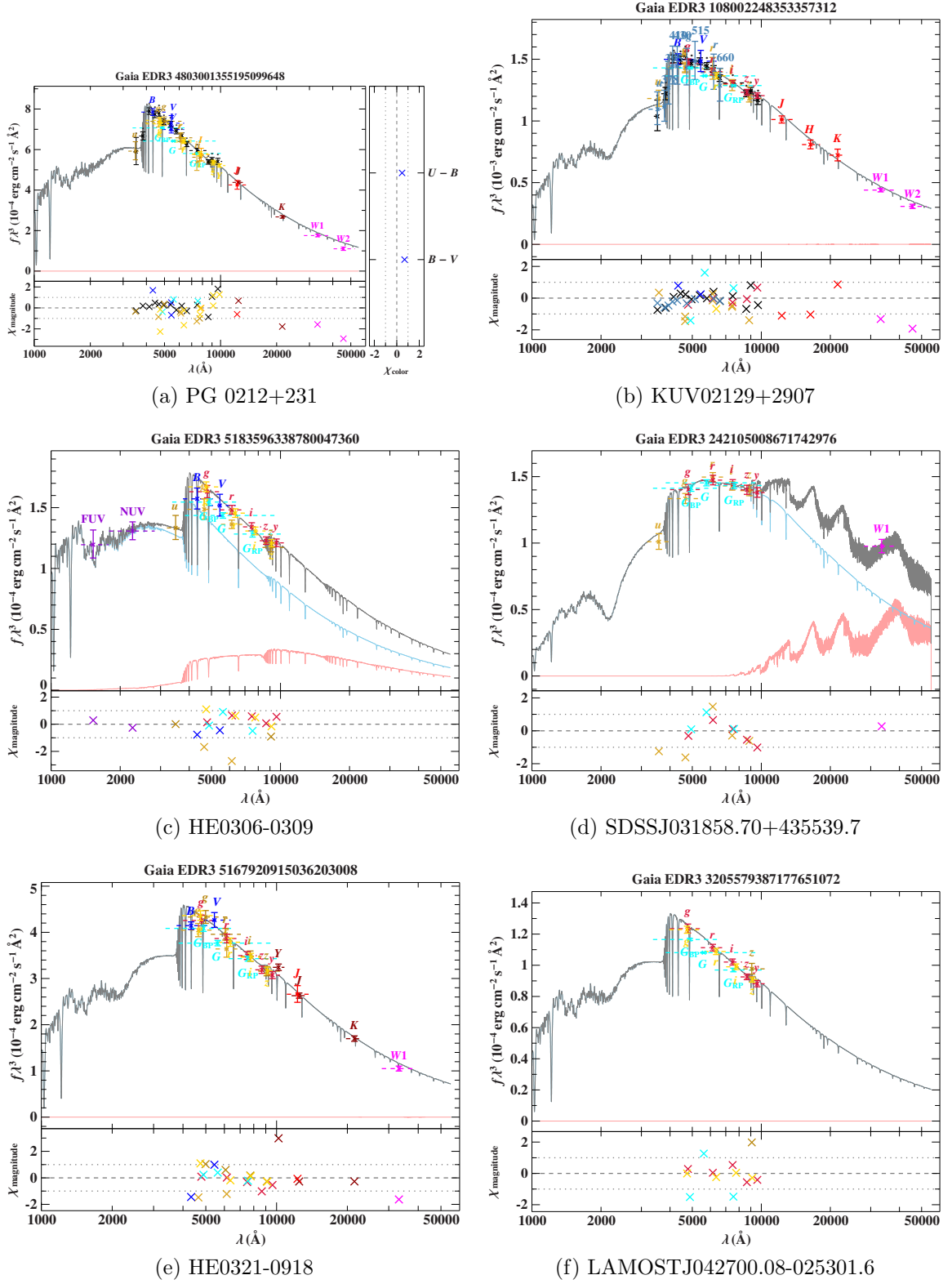


Figure 27: SEDs 1/6

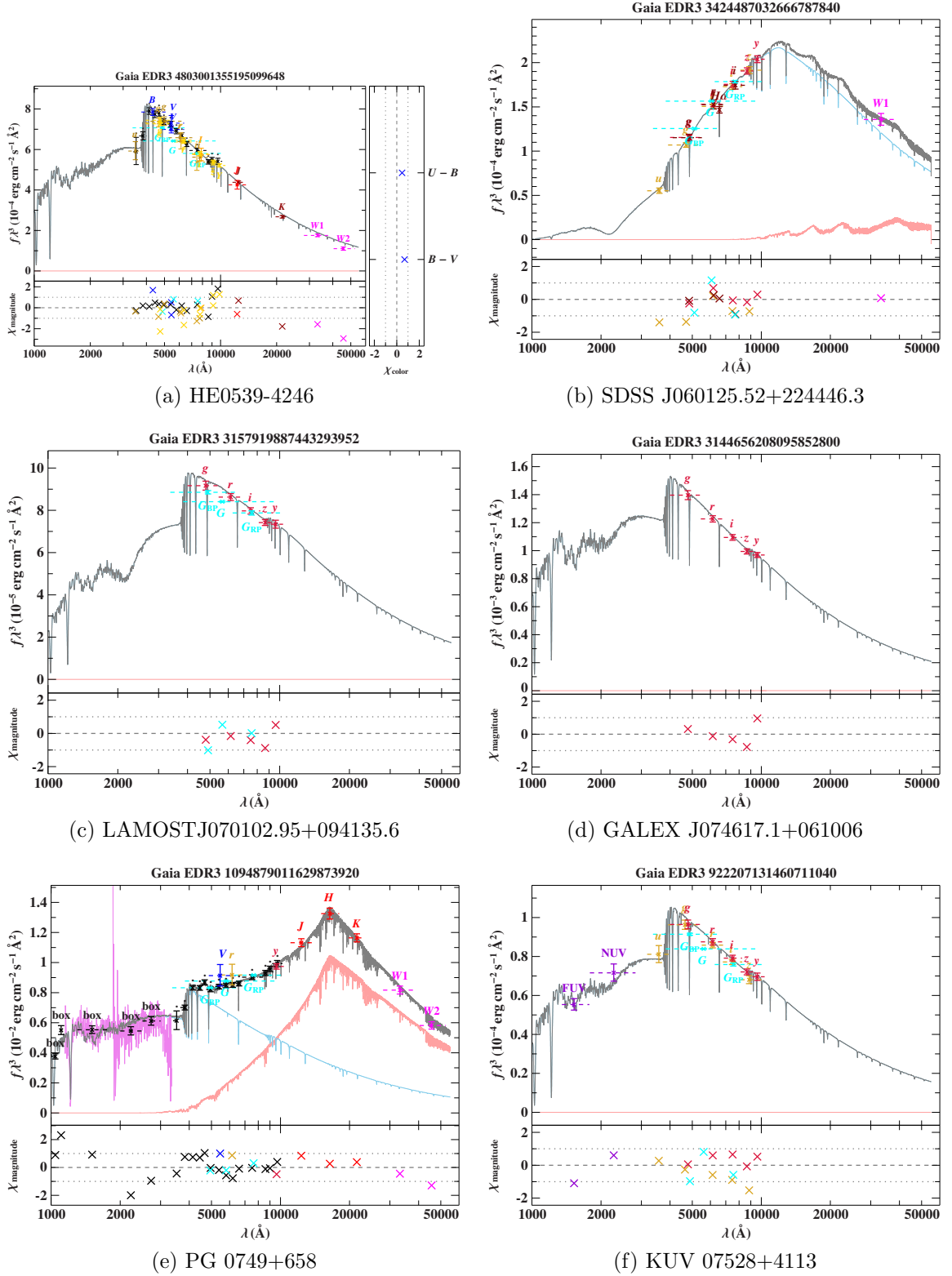


Figure 28: SEDs 2/6

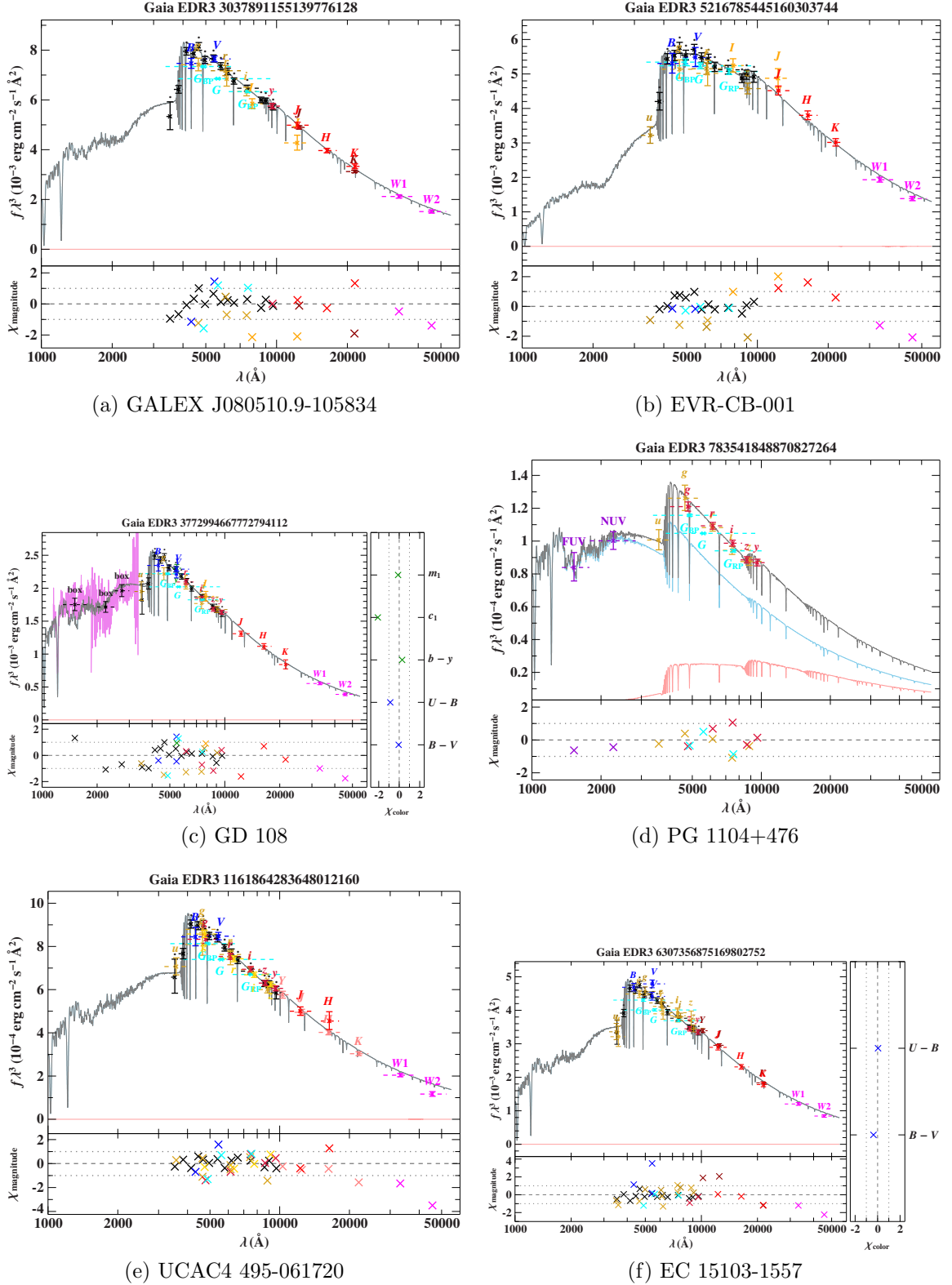


Figure 29: SEDs 3/6

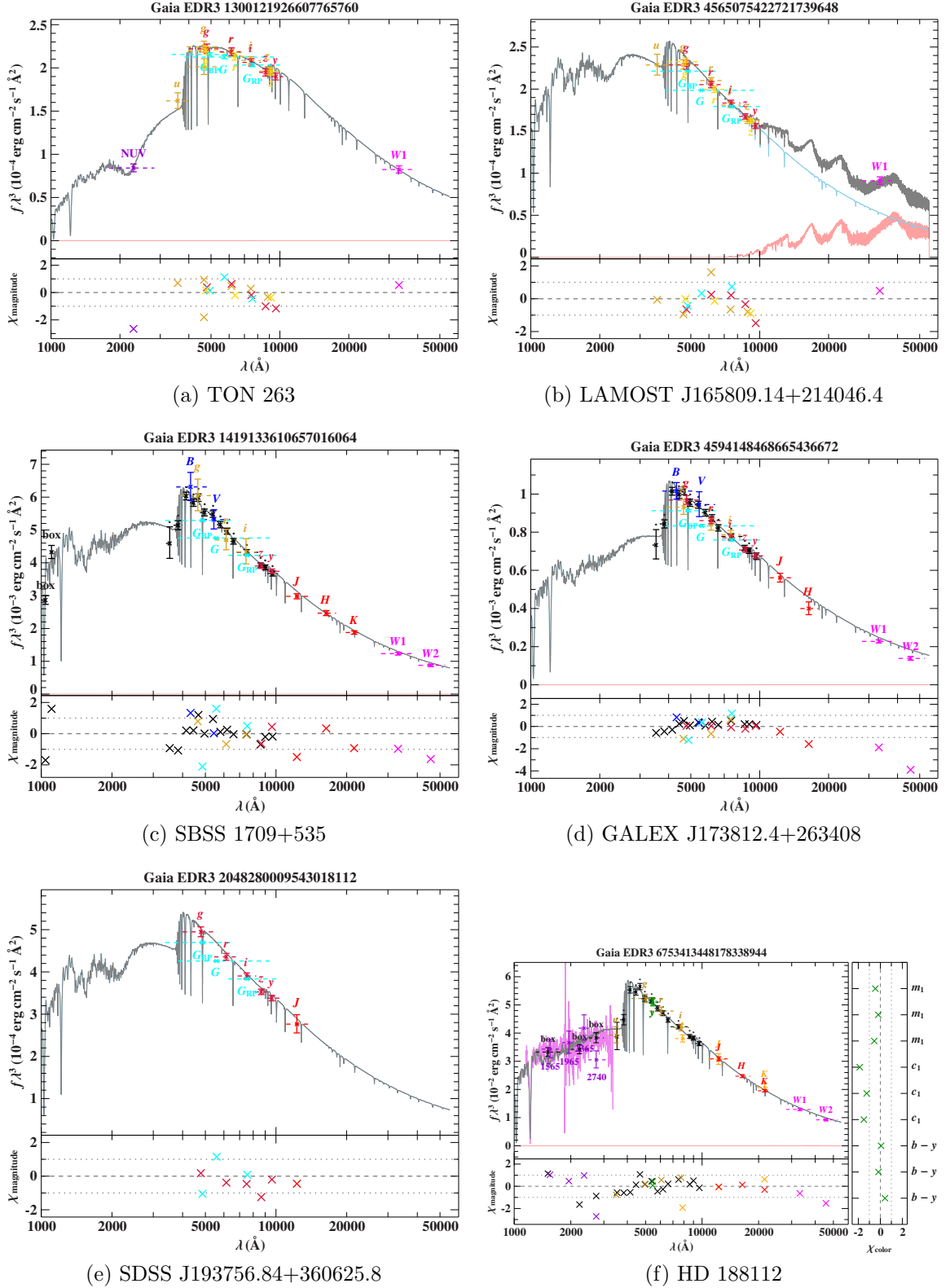


Figure 30: SEDs 4/6

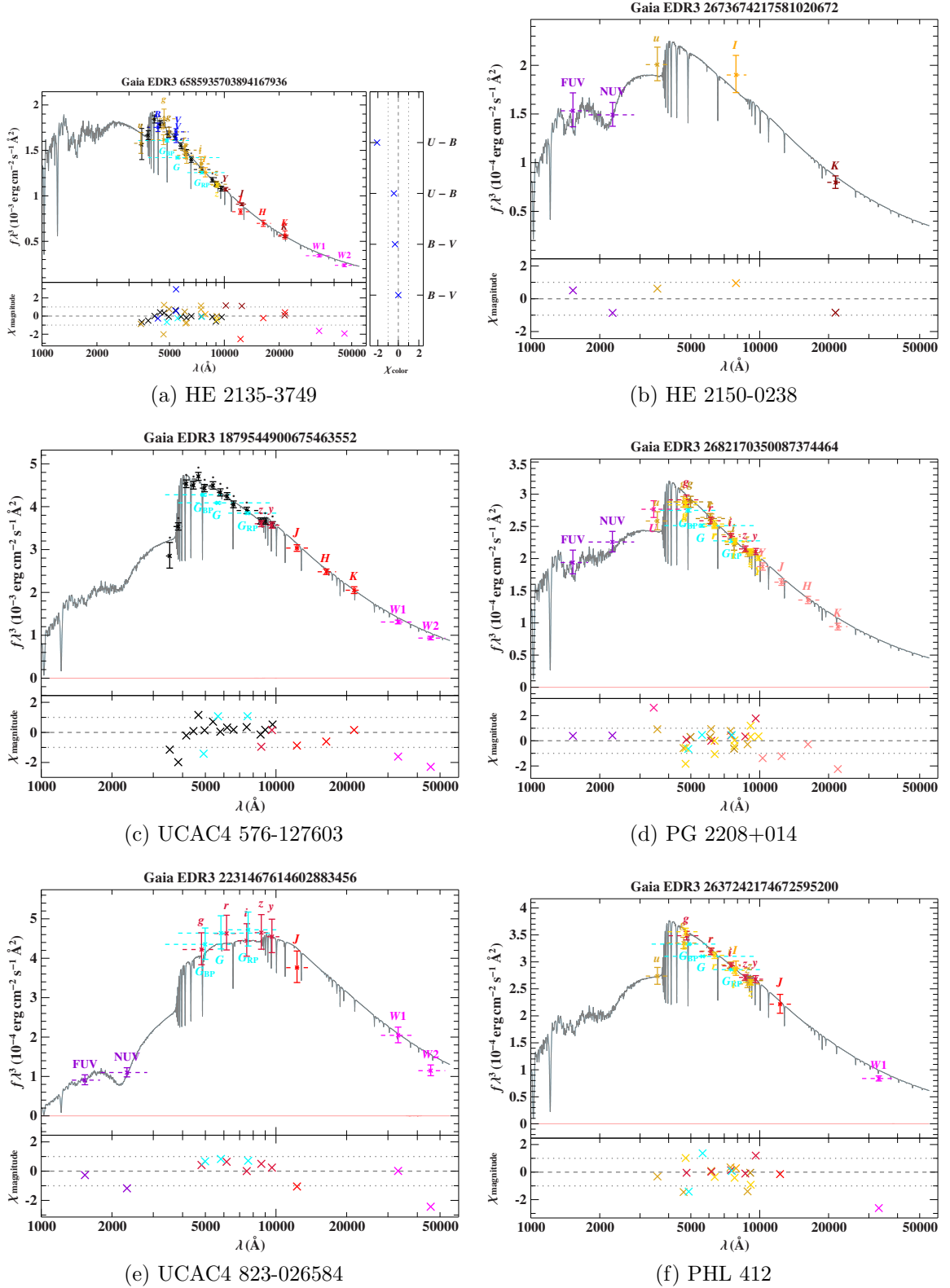
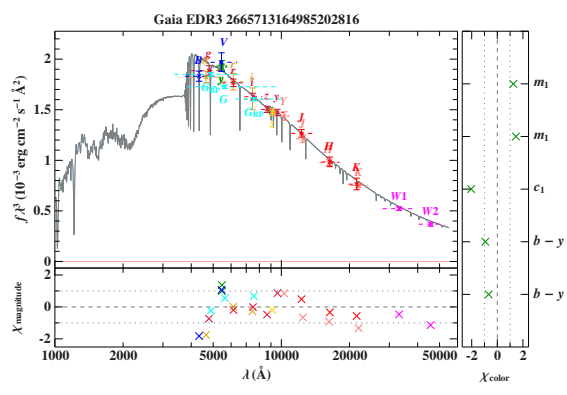


Figure 31: SEDs 5/6



(a) Feige 109

Figure 32: SEDs 6/6

Declaration of self-commitment

Hereby I declare that I wrote this work on my own and without using foreign support. Sources are indicated when I used information from others.
This work has neither been submitted to any examination authority nor has it been published yet.

Potsdam, 14 October 2022

Henry Willems